

Solution of the Multi-Channel Anderson Impurity Model – Ground State and Thermodynamics –

C. J. Bolech^{1,2}

¹ *Département de Physique de la Matière Condensée, Université de Genève,
Quai Ernest Ansermet 24, CH-1211 Genève 4, Switzerland*

N. Andrei²

² *Center for Materials Theory, Serin Physics Laboratory, Rutgers University,
136 Frelinghuysen Road, Piscataway, New Jersey 08854-8019, USA*

(Dated: July 14th, 2004)

We present the solution of the $SU(N) \otimes SU(M)$ Anderson impurity model using the Bethe-Ansatz. We first explain what extensions to the formalism were required for the solution. Subsequently we determine the ground state and derive the thermodynamics over the full range of temperature and fields. We identify the different regimes of valence fluctuation at high temperatures, followed by moment formation or intrinsic mixed valence at intermediate temperatures and a low temperature non-Fermi liquid phase. Among other things we obtain the impurity entropy, charge valence, and specific heat over the full range of temperature. We show that the low-energy physics is governed by a line of fixed points. This describes non-Fermi-liquid behavior in the integral valence regime, associated with moment formation, as well as in the mixed valence regime where no moment forms.

I. INTRODUCTION

Heavy-fermion materials have been a source of interest and puzzlement since the experimental discovery of superconductivity in CeCu_2Si_2 in 1979.¹ By the turn of the 1990s the non-Fermi liquid character of these materials was coming to the center of attention (for a recent review see Ref. [2]), coincidentally with the interest on marginal Fermi liquids generated by the normal state of high- T_c superconductors. Since then, the number of examples of violation of Landau's Fermi liquid theory among lanthanides and actinides has multiplied.

Current theories trying to explain the non-Fermi liquid behavior in d- and f-electron metals can be classified into three broad categories: (i) models based on multi-channel Kondo physics, (ii) models considering the proximity of a quantum critical point, and (iii) models based on single-channel Kondo physics but in the presence of disorder that induces a distribution of impurity energy scales. These three ingredients are not mutually exclusive and a number of recent theories try to address their effects in different combinations (see [2] for references). In this article we will be concerned with the first class of models. This approach originated with the work of Cox,³ in turn motivated by the unusual experimental results in the heavy-fermion compound UBe_{13} .⁴ He argued that the notably weak magnetic field dependence of the specific heat of this material excludes the usual magnetic Kondo effect and proposed instead that the observed anomalous behavior derives from the quenching of quadrupolar degrees of freedom. In this case, the spin of the conduction band electrons plays the role of a channel degree of freedom. This is the two-channel quadrupolar Anderson model, describing tetravalent uranium impurities in a cubic-symmetric metallic matrix. The model was later generalized to include other crystal symmetries as well as more complicated crystal field splittings; for a review see

Ref. [5]. In more detail, Hund's rules and spin-orbit coupling in the presence of a cubic crystalline electric field lead to the modeling of a U ion in a Be_{13} host by a Γ_6 Kramers doublet in a $5f^3$ configuration and a quadrupolar (nonmagnetic) doublet Γ_3 in the $5f^2$ configuration. The doublets hybridize with conduction electrons in a Γ_8 representation carrying both spin and quadrupolar quantum numbers. This single-impurity approach was not uncontroversial.^{6,7} For instance, whether the energy splitting between the two doublets is sufficiently large for a quadrupolar Kondo scenario to be viable is still largely unresolved. Aliev *et al.* presented experimental evidence suggesting that both doublets may in fact be nearly degenerate, pointing to a mixed-valent state with a novel type of interplay between magnetic and quadrupolar two-channel type screening.⁸

In this article we will study the general multi-channel Anderson impurity model that includes as particular cases the two-channel model and, to some extent, most of its generalizations alluded to above.⁵ The so-called $SU(N) \otimes SU(M)$ Anderson impurity model, in its pseudo-particle representation, is given by the following Hamiltonian:

$$H_{\text{MchA}} = H_{\text{host}} + \varepsilon_q \sum_{\alpha} b_{\alpha}^{\dagger} b_{\bar{\alpha}} + \varepsilon_s \sum_{\sigma} f_{\sigma}^{\dagger} f_{\sigma} + \\ + V \sum_{\bar{\alpha}, \sigma} \left[f_{\sigma}^{\dagger} b_{\bar{\alpha}} \psi_{\alpha, \sigma}(0) + \psi_{\alpha, \sigma}^{\dagger}(0) b_{\bar{\alpha}}^{\dagger} f_{\sigma} \right]$$

subject to the constraint: $\sum_{\alpha} b_{\alpha}^{\dagger} b_{\bar{\alpha}} + \sum_{\sigma} f_{\sigma}^{\dagger} f_{\sigma} = 1$. The first term in the Hamiltonian describes the host in which the impurity is embedded. For our purposes, we model it as a linearized Fermi band,

$$H_{\text{host}} = \sum_{\alpha, \sigma} \int \psi_{\alpha, \sigma}^{\dagger}(x) (-i \partial_x) \psi_{\alpha, \sigma}(x) dx.$$

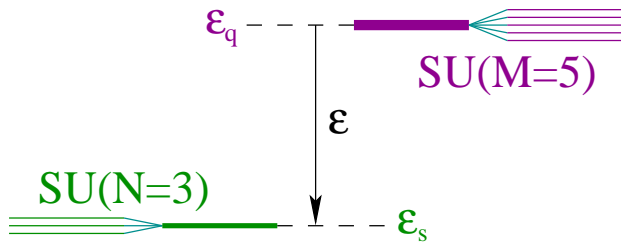


FIG. 1: Impurity level scheme for the case of an Anderson model with a three-fold degenerate magnetic configuration of energy ϵ_s and a five-fold degenerate quadrupolar one of energy ϵ_q . The energy difference $\epsilon = \epsilon_s - \epsilon_q$ is indicated with an arrow.

The second and third terms model two multiplets with energies ϵ_s and ϵ_q and quantum numbers $\sigma \in SU(N)$ and $\bar{\alpha} \in SU(M)$, respectively.⁶⁹ We will refer to this two quantum numbers as generalized spin and flavor – in reference to the Kramers (magnetic) and non-Kramers (quadrupolar) doublets of the two-channel case. The last term in the Hamiltonian describes the hybridization of the host electrons with the impurity.

An illustrative level scheme is given in Fig. 1 where the magnetic configuration is taken to lie lower in energy than the quadrupolar one. The particular example is for an Anderson model with $SU(N=3) \otimes SU(M=5)$ symmetry. The impurity can switch between the two configurations by giving or taking an electron from the host band, a process that takes place with an overlap amplitude given by V .

As a result of the constraint, the impurity Hilbert space is restricted to $N + M$ states. Namely, N flavorless spin states $|\sigma\rangle \equiv f_\sigma^\dagger |0\rangle$ plus M spinless flavor states $|\bar{\alpha}\rangle \equiv b_{\bar{\alpha}}^\dagger |0\rangle$. Defining these states explicitly, we can rewrite the Hamiltonian in a different notation that automatically accounts for the Hilbert space restriction,

$$H_{\text{MchA}} = H_{\text{host}} + \epsilon_q \sum_{\bar{\alpha}} |\bar{\alpha}\rangle \langle \bar{\alpha}| + \epsilon_s \sum_{\sigma} |\sigma\rangle \langle \sigma| + V \sum_{\alpha, \sigma} [\sigma\rangle \langle \bar{\alpha}| \psi_{\alpha, \sigma}(0) + \psi_{\alpha, \sigma}^\dagger(0) |\bar{\alpha}\rangle \langle \sigma|].$$

Both forms of the Hamiltonian are completely equivalent when the constraint is treated exactly and both are widely used in the literature.⁵ It is the constraint acting in the Hilbert space that plays the role of a strong interaction and renders the problem highly non-perturbative.

As a side remark notice that if either M or N is put to one, the model reduces to a degenerate single-channel Anderson model in the limit of infinite Coulomb repulsion (a magnetic or a quadrupolar version of it, respectively).^{9,10} While the standard single-channel $SU(2)$ Anderson model¹¹ was found to be integrable,^{12,13} its $SU(N)$ generalization is not integrable except for the strong repulsion limit when the impurity is constrained not to exceed single occupancy.^{14,15}

Even though the multi-channel Anderson model was put forward more than fifteen years ago, progress in its theoretical understanding has been slow. In the two-channel case ($N = M = 2$) most of the early knowledge of its unusual physics came from the integer valence limit. In this limit the model maps onto the two-channel Kondo model for which the Bethe-Ansatz solution was available.^{16,17,18} Also Numerical Renormalization Group (NRG)^{19,20} and Boundary Conformal Field Theory (BCFT)²¹ studies were carried out. Only more recently some progress was made in the study of the mixed valence regime of the two-channel Anderson model using Monte Carlo²² and NRG^{23,24} methods. The more general multi-channel case is, however, not quite within the present reach of NRG and other approaches. On the other hand, the large N and M case constitutes the natural starting point for alternative approaches like the Non-Crossing Approximation (NCA),^{22,25} the *conserving slave boson theory*,^{26,27} or other types of $1/N$ -expansions.²⁸ Since the general multi-channel Anderson model can be regarded as the extension of the infinitely-repulsive degenerate single-channel Anderson model to the multi-channel case, the question about its integrability arises naturally. During the last couple of years the integrability was established, opening up the possibility of a full understanding of the model. In previous work, we presented the Bethe-Ansatz solution for the two-channel case.²⁹ Subsequently, we developed the critical low-energy theory of that model using BCFT and combining it with results from Thermodynamic Bethe-Ansatz.^{30,31}

A. Preview of Main Results

In the present work we will give a detailed and, to a large extent, self-contained account of the Bethe-Ansatz solution of the general multi-channel Anderson model. We shall show that, as in the case of the two channel model, the low energy physics of the impurity is governed by a line of boundary fixed points with a non-trivial residual impurity entropy that is constant along the line. We shall identify two energy scales (T_H and T_L) that govern the screening process of the impurity degrees of freedom. The screening occurs in two stages parameterized by these scales as will be seen, for instance, in the temperature dependence of the impurity entropy. The mixed valence regime will be discussed in detail, stressing not only the differences, but also the unexpected similarities with the integer valence cases.

In Fig. 2 we present the picture that emerges for the different regimes of the model. As a function of temperature and energy difference between impurity configurations ($\epsilon = \epsilon_s - \epsilon_q$), we will characterize the different regimes (FV, LMM and LQM, and FP; see figure caption). In particular, moment formation takes place (for a fixed and suitably large ϵ) as the temperature falls below T_H ; the moment being magnetic or quadrupolar depending on the sign of ϵ . It is then screened as T is further

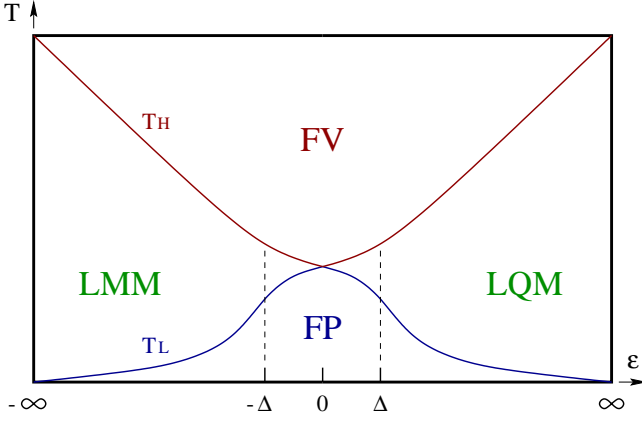


FIG. 2: Schematic representation of the two temperature scales indicating the crossovers among different regimes: fluctuating valence (FV), fixed point (FP), and local magnetic and quadrupolar moment regimes (LMM and LQM).

lowered below T_L when the system is governed by the infrared fixed point. Notice that the moment formation region becomes smaller as $|\varepsilon|$ is reduced and completely disappears at $\varepsilon \simeq 0$. In fact, over the whole mixed valence region ($|\varepsilon| \lesssim \Delta \equiv V^2/2$), valence fluctuations suffice to prevent moment formation.

Another way of presenting the picture is to define two energy scales (T_s and T_q) associated with the spin and quadrupolar degrees of freedom. These scales cross each other in the intermediate valence region and interchange roles as the high-temperature (T_H) and low-temperature (T_L) scales that indicate the transition zones among different regimes. The meeting of the two scales in the intermediate valence region signals the absence of a moment formation regime between the high and the low temperatures: the fixed point is reached *without* prior moment formation.

The rest of this article is organized as follows: in the next section we will discuss the scattering matrices and the integrability of the model (Sec. II); in the subsequent one we will present some necessary formal developments in the theory of quantum inverse scattering and the equations derived from them (Sec. III); in the following two we will discuss the thermodynamics of the model – we shall give formal derivations (Sec. IV) and analytic and numerical results (Sec. V) –; in the last section we will provide a summary and a discussion of our main results as well as an outlook of their applications in the theory of heavy fermions (Sec. VI).

II. S-MATRICES AND INTEGRABILITY

The Hamiltonian H_{MchA} conserves the number of fermionic excitations (electrons),

$$N_e = \sum_{\alpha, \sigma} \int \psi_{\alpha, \sigma}^\dagger(x) \psi_{\alpha, \sigma}(x) + \sum_{\sigma} f_{\sigma}^\dagger f_{\sigma}$$

allowing us to study the system for an arbitrary but fixed value of N_e . We take $N_e = 0$ as our reference sector, an M -degenerate eigenstate with energy ε_q . Our strategy will be the usual one in coordinate Bethe-Ansatz: we solve the system for $N_e = 1, 2, \dots$ and then generalize the solution to arbitrary values of N_e . Subsequently, as the $N_e \rightarrow \infty$ limit is taken (discussed in later sections), the field theory is recovered.

A. Electron-Impurity Scattering Matrix

When there is only one electron present in the system ($N_e = 1$), the most general one-fermion state has the following form:

$$|k\rangle = \sum_{\alpha, \beta, \sigma} \int F_{\alpha\sigma; \beta}^k(x) \psi_{\alpha\sigma}^\dagger(x) |\bar{\beta}\rangle + G_{\sigma}^k |\sigma\rangle.$$

To determine the eigenstates of the Hamiltonian in this sector, satisfying $H|k\rangle = E^k|k\rangle$, we apply the Hamiltonian to this generic state and derive the *first quantized Schrödinger equations* in the sector. Using the expression $E^k = k + \varepsilon_q$ for the eigenenergies of eigenstates $|k\rangle$, we read off the equations:

$$\begin{cases} (-i\partial_x - k) F_{\alpha\sigma; \beta}^k(x) + \delta(x) V \delta_{\alpha}^{\beta} G_{\sigma}^k = 0 \\ (\varepsilon - k) G_{\sigma}^k + \sum_{\alpha', \beta'} V \delta_{\alpha'}^{\beta'} F_{\alpha'\sigma; \beta'}^k(0) = 0 \end{cases}$$

where the energy difference $\varepsilon = \varepsilon_s - \varepsilon_q$ was introduced. We call $F_{\alpha\sigma; \beta}^k(x)$ and G_{σ}^k the wavefunctions. Eliminating G_{σ}^k from the first equation and setting $F_{\alpha\sigma; \beta}^k(x) = e^{ikx} \tilde{F}_{\alpha\sigma; \beta}^k(x)$ we have (repeated indexes are summed over)

$$(k - \varepsilon) (-i\partial_x) \tilde{F}_{\alpha\sigma; \beta}^k(x) + V^2 \delta(x) \delta_{\alpha}^{\beta} \delta_{\alpha'}^{\beta'} \tilde{F}_{\alpha'\sigma; \beta'}^k(0) = 0.$$

We make the following Bethe-type ansatz for the coordinate dependence of the \tilde{F} -wavefunction: $\tilde{F}_{\alpha\sigma; \beta}^k(x) = [(\theta(-x)\mathbf{I} + \theta(x)\mathbf{S})A]_{\alpha\sigma; \beta}^k$, where \mathbf{S} will be called the electron-impurity scattering matrix and A is an arbitrary vector in the internal space of the one-electron sector. In order to fully define the ansatz we adopt the following convention for the step function: $\theta(0) = 1/2$. Let us introduce the operator $[\mathbf{Q}]_{\alpha; \beta}^{\alpha'; \beta'} = \delta_{\alpha}^{\beta} \delta_{\alpha'}^{\beta'}$ that acts in flavor space and has the property $\mathbf{Q}^2 = M\mathbf{Q}$ (recall M is the number of values that the index α takes). Since A is arbitrary, one has a matrix equation for \mathbf{S} . Its solution is

$$\begin{aligned} \mathbf{S}_{1,0} &= \mathbf{I}_{1,0} - \frac{i2V^2}{2(k_1 - \varepsilon) + iMV^2} \mathbf{Q}_{1;0} \\ &= \mathbf{I}_{1,0} + \frac{e^{-i\delta(k_1 - \varepsilon)} - 1}{M} \mathbf{Q}_{1;0}, \end{aligned}$$

where we used the index ‘1’ for the only electron present in the system and introduced the use of the index ‘0’

for the impurity (the notation $k_0 \equiv \varepsilon$ will be also used latter). For the second way of writing $\mathbf{S}_{1,0}$ we introduced the phase $\delta(k - \varepsilon) = 2 \arctan \frac{MV^2}{2(k - \varepsilon)}$.

It is easy to verify unitarity,

$$\mathbf{S}\mathbf{S}^\dagger = \mathbf{S}_{1,0}\mathbf{S}_{0,1} = \mathbf{I}.$$

$$|k_1 k_2\rangle = \int \int F_{\alpha_1 \sigma_1 \alpha_2 \sigma_2; \beta}^{k_1 k_2}(x_1, x_2) \psi_{\alpha_1 \sigma_1}^\dagger(x_1) \psi_{\alpha_2 \sigma_2}^\dagger(x_2) |\bar{\beta}\rangle + \int G_{\alpha_1 \sigma_1; \sigma_2}^{k_1 k_2}(x_1) \psi_{\alpha_1 \sigma_1}^\dagger(x_1) |\sigma_2\rangle.$$

Now again we apply the Hamiltonian in order to obtain the first quantized Schrödinger equations for eigenstates with eigenenergies $E^{k_1 k_2} = k_1 + k_2 + \varepsilon_q$. We arrive at the following set of differential equations:

$$\begin{cases} \sum_{n=1,2} (-i\partial_{x_n} - k_n) [\mathcal{A}F]_{\alpha_1 \sigma_1 \alpha_2 \sigma_2; \beta}^{k_1 k_2}(x_1, x_2) + V \mathcal{A} [\delta(x_2) \delta_{\alpha_2}^\beta G_{\alpha_1 \sigma_1; \sigma_2}^{k_1 k_2}(x_1)] = 0 \\ (-i\partial_{x_1} - k_1 + \varepsilon - k_2) G_{\alpha_1 \sigma_1; 0 \sigma_2}^{k_1 k_2}(x_1) + V \delta(x_2) \delta_{\alpha_2}^\beta [\mathcal{A}F]_{\alpha_1 \sigma_1 \alpha_2 \sigma_2; \beta}^{k_1 k_2}(x_1, x_2) = 0 \end{cases}$$

where $\mathcal{A} = \mathbf{I} - \mathbf{P}^{xsq} = \mathbf{I} - \mathbf{P}^x \mathbf{P}^s \mathbf{P}^q$ is (twice) the antisymmetrizer in coordinate, spin, and (quadrupolar)-flavor space, expressed in terms of $\mathbf{P}^x, \mathbf{P}^s, \mathbf{P}^q$ the permutation operators that act in the spaces indicated.

Now we make an ansatz for the F -wavefunction similar in spirit to the one we made in the one-electron sector. There are six regions in configuration space, corresponding to the six possible line arrangements of the impurity and the two electrons. The region with, say, electron ‘1’ to the immediate left of the impurity is related via the S-matrix $\mathbf{S}_{1,0}$ to the region with electron ‘1’ to the immediate right (the position of electron ‘2’ remains un-

changed). A similar role is played by $\mathbf{S}_{2,0}$. However, we still need to determine how to relate the regions where electrons ‘1’ and ‘2’ exchange places (away from the impurity).

Consider then,

$$F_{\alpha_1 \sigma_1 \alpha_2 \sigma_2; \beta}^{k_1 k_2}(x_1, x_2) = e^{ik_1 x_1 + ik_2 x_2} \tilde{F}_{\alpha_1 \sigma_1 \alpha_2 \sigma_2; \beta}^{k_1 k_2}(x_1, x_2)$$

with the expression for \tilde{F} describing the six different arrangements of particles,

$$\begin{aligned} \tilde{F}_{\alpha_1 \sigma_1 \alpha_2 \sigma_2; \beta}^{k_1 k_2}(x_1, x_2) = & [(\theta(x_{12}) \theta(-x_2) \mathbf{I} + \theta(x_{21}) \theta(-x_1) \mathbf{S} + \theta(-x_1) \theta(x_2) \mathbf{S}_{2,0} + \\ & + \theta(-x_2) \theta(x_1) \mathbf{S}_{1,0} \mathbf{S} + \theta(x_1) \theta(x_{12}) \mathbf{S}_{1,0} \mathbf{S}_{2,0} + \theta(x_2) \theta(x_{21}) \mathbf{S}_{2,0} \mathbf{S}_{1,0} \mathbf{S}) A]_{\alpha_1 \sigma_1 \alpha_2 \sigma_2; \beta}^{k_1 k_2}. \end{aligned}$$

Here $\mathbf{S}_{1,0}$ and $\mathbf{S}_{2,0}$ are the electron-impurity S-matrices found above and $\mathbf{S} \equiv \mathbf{S}_{1,2}$ is the electron-electron S-matrix that we seek to determine in this subsection. As above A is an arbitrary vector in the internal space of the two-electron sector, determining the state of two electrons and the impurity. To define unambiguously the ansatz we adopt the regularization $\theta(0^-) \theta(0^+) \stackrel{\text{def}}{=} 0$,⁷⁰ consistent with the first order character of the differential equations. Let us mention that this ansatz assumes that the same momenta k_1, k_2 characterize the wavefunction in all six regions (*i.e.* orderings). This is at the heart of the ansatz and will be shown to be valid later when we discuss the Yang-Baxter conditions.

Inserting the wavefunction into the first of the Schrödinger equations above we verify after some algebra that the equation holds, determining uniquely the form of the G -wavefunction. At this stage the electron-electron scattering matrix remains arbitrary and we turn our attention to the second Schrödinger equation. Carrying out the algebra, we find that the equation holds provided the following matrix constraint on the electron-electron S-matrix is obeyed:

$$(\mathbf{S}_{2,0} - \mathbf{I})(\mathbf{S}_{1,0} \mathbf{S} - \mathbf{I}) - \mathbf{P}^{qs}(\mathbf{S}_{1,0} - \mathbf{I})(\mathbf{S}_{2,0} - \mathbf{S}) = \mathbf{0}$$

where the matrices without indexes act on the internal space of the two electrons. A careful examination of this equation reveals the presence of an overall left-prefactor

$\mathbf{Q}_{2,0}$. Since this operator is not invertible, the solution of the constraint is not unique and there is still a certain amount of freedom left in the choice of \mathbf{S} .

1. An Integrable Solution

The equation above does not have a unique solution for the two-electron S-matrix \mathbf{S} . For our purpose we need to identify, however, a particular solution having the appropriate physical properties that ensure the generalization and consistency of the ansatz to any number of electrons N_e . These requirements are:

Unitarity Condition	$\mathbf{S}_{ij}\mathbf{S}_{ji} = \mathbf{I}$
Locality of the Scattering	$\mathbf{S}_{ij}\mathbf{S}_{kl} = \mathbf{S}_{kl}\mathbf{S}_{ij}$
Yang-Baxter Relation	$\mathbf{S}_{jk}\mathbf{S}_{ik}\mathbf{S}_{ij} = \mathbf{S}_{ij}\mathbf{S}_{ik}\mathbf{S}_{jk}$

TABLE I: Three necessary conditions for integrability.

The first of these relations assures the reversibility of the scattering processes (or reversibility of the scattering paths) and the other two are enough to guarantee path independence for arbitrary N_e .^{32,33} With these conditions, any multiparticle scattering process can be factorized into pairwise scattering events and there is no ambiguity in the multiple ways of carrying out the factorization since they are all equivalent (the reader can find an illustration of the situation in four-particle space in the review article of Ref. [34]). We remark that in the case of impurity models, any one of the indices in these relations can take the value ‘0’ that stands for the impurity.

These three conditions together with the constraint coming from the Schrödinger equation, constitute an over-constrained algebraic system for determining the electron-electron S-matrix ($\mathbf{S} \equiv \mathbf{S}_{1,2}$). Nevertheless, it admits a solution.

It can be shown that the only solution is the following:

$$\mathbf{S}_{1,2} = \frac{(k_1 - k_2) - iV^2 \mathbf{P}_{1,2}^s (k_1 - k_2) + iV^2 \mathbf{P}_{1,2}^q}{(k_1 - k_2) - iV^2 (k_1 - k_2) + iV^2}.$$

This matrix serves to describe the electron band with linear dispersion within a basis of reduced symmetry $SU(NM) \rightarrow SU(N) \otimes SU(M)$, consistent with the reduction in symmetry operated by the addition of the impurity terms to the Hamiltonian of the host band. It is important to emphasize that the introduction of $\mathbf{S}_{1,2}$ does not signify that we have modified the original Hamiltonian H_{MchA} by introducing electron-electron interaction. Instead, the choice of $\mathbf{S}_{1,2}$ corresponds to a choice of basis in the space of free electrons.⁷¹

III. PERIODIC BOUNDARY CONDITIONS AND BETHE-ANSATZ EQUATIONS

We proceed to impose boundary conditions. This is required in order to be able to properly count and label the

states. We will discuss here the case of periodic boundary conditions, imposing the following set of conditions on the N_e -electron wave function,

$$F_{\{\vec{m}\}}^{\{k\}}(\{x\}) \Big|_{x_j = \frac{L}{2}} = F_{\{\vec{m}\}}^{\{k\}}(\{x\}) \Big|_{x_j = -\frac{L}{2}}$$

where we are considering a finite ring of length L . As we are able to move electron j to the far left ($x_j = -L/2$) or to the far right ($x_j = L/2$) using the S-matrices, the boundary condition gives rise to the following eigenvalue problem:

$$Z_j \vec{A} = z_j \vec{A}$$

where the eigenvalues $z_j = e^{-ik_j L}$ of the transfer matrix Z_j ,

$$Z_j = S_{jj-1} \dots S_{j1} S_{j0} S_{jN} \dots S_{jj+1}$$

will allow us to find the spectrum of the Hamiltonian via $E = \sum k_j$. \vec{A} is a vector in the internal space of the N_e electron sector. Equivalently, this condition corresponds to taking particle j *around the ring* and asking that the wave function should not change; it should hold for all $j = 1, \dots, N_e$. The original problem of finding the eigenenergies and eigenfunctions of the Hamiltonian is thus reduced to that of finding the vector amplitudes in internal space (\vec{A}) that are simultaneous eigenvectors of all these eigenvalue problems.

The solution of this class of eigenvalue problems was first tackled by Yang,³³ who solved the problem by means of a ‘second Bethe-Ansatz’ (see also the work of Baxter³⁵). In the late 1970s the procedure was systematized into what is known as the *Quantum Inverse Scattering Method* (QISM).³⁶ However, the existing technology is insufficient for our purpose; the structure of the impurity S-matrix in the multi-channel Anderson model requires a reformulation and extension of the standard formalism. We give a detailed account of those developments in one of the appendices at the end of the article.

A. Bethe-Ansatz Equations for the Multi-Channel Anderson Impurity Model

The eigenvalues, $z_j = e^{-ik_j L}$, of the transfer matrix are given in terms of the *charge rapidities* (k_j), which in their turn, together with the *spin rapidities* ($\Lambda_\alpha^{s(r)}$) and the *quadrupolar-flavor rapidities* ($\Lambda_\alpha^{q(r)}$), completely specify the particular eigenstate (see first appendix). The spin rapidities ($\Lambda_\alpha^{s(r)}$) and the q-flavor rapidities ($\Lambda_\alpha^{q(r)}$) describe, respectively, the spin and flavor dynamics as well as the symmetry of each state. The index $x = s, (q)$ specifies that $\Lambda_\alpha^{x(r)}$ refers to a spin (q-flavor) degree of freedom, the index r describes the *rank* (related to the spin or flavor symmetry of the state), and finally α labels the different rapidities of each type and rank.

The charge, spin, and flavor rapidities must satisfy a set of equations - the Bethe-Ansatz Equations (BAE) -

that are derived in the first appendix. These equations encode the full information of the model:

$$e^{ik_j L} = \prod_{n=1}^{M_1^s} \frac{k_j - \Lambda_n^{s(1)} - i\Delta}{k_j - \Lambda_n^{s(1)} + i\Delta} \prod_{m=1}^{M_1^q} \frac{k_j - \Lambda_m^{q(1)} + i\Delta}{k_j - \Lambda_m^{q(1)} - i\Delta}$$

with the conditions,

$$\prod_{m \neq n}^{M_r^s} \frac{\Lambda_n^{s(r)} - \Lambda_m^{s(r)} - i2\Delta}{\Lambda_n^{s(r)} - \Lambda_m^{s(r)} + i2\Delta} = \prod_{\substack{m=1 \\ \sigma=\pm 1}}^{M_{r+\sigma}^s} \frac{\Lambda_n^{s(r)} - \Lambda_m^{s(r+\sigma)} - i\Delta}{\Lambda_n^{s(r)} - \Lambda_m^{s(r+\sigma)} + i\Delta}$$

$$\prod_{m \neq n}^{M_r^q} \frac{\Lambda_n^{q(r)} - \Lambda_m^{q(r)} - i2\Delta}{\Lambda_n^{q(r)} - \Lambda_m^{q(r)} + i2\Delta} = \prod_{\substack{m=1 \\ \sigma=\pm 1}}^{M_{r+\sigma}^q} \frac{\Lambda_n^{q(r)} - \Lambda_m^{q(r+\sigma)} - i\Delta}{\Lambda_n^{q(r)} - \Lambda_m^{q(r+\sigma)} + i\Delta}$$

where for convenience we have used the definitions,

$$\Lambda_n^{s,q(0)} = k_n$$

$$\Lambda_1^{q(M)} = \varepsilon$$

and accordingly $M_0^{s,q} = N_e$, $M_M^q = N_i = 1$, and $M_N^s = 0$. One sees that the effect of the impurity enters via the auxiliary conditions for the *q-flavor rapidities*. This is a distinguishing feature, different from what happens in the equations for the single-channel Anderson model, or in those for the Kondo model regardless of the number of channels.

Each solution of the BAE corresponds to an eigenstate of the Hamiltonian. The eigenfunction can in principle be determined from the eigenvector \vec{A} and the corresponding energy eigenvalue is given by

$$E = \sum_j k_j .$$

The charge-, spin- and quadrupolar-rapidities entering the solutions of the BAE are in general complex, and take the form, in the thermodynamic limit, of *strings*.^{37,38,39} An *n*-string of spin or q-flavor rapidities consists of *n* equally spaced complex numbers symmetrically arranged around the real axis ($x = s, q$):

$$\Lambda_{n\sigma}^{x(r)} = \Lambda_n^{x(r)} + i(n+1-2\sigma)\Delta \quad \text{with } \sigma = 1, \dots, n .$$

Strings are thus specified by a single real number $\Lambda_n^{x(r)}$, in terms of which we shall rewrite the BAE. Similarly, there also complex values of the charge rapidities k_j corresponding to bound states among the bare electrons that build up the theory. They too form strings and will be incorporated in the BAE through the real part characterizing them. Consider a bound state of *n* particles, the corresponding charge rapidities form a string:

$$k_\sigma^{(0)} = k^{(n-1)} + i(n+1-2\sigma)\Delta \quad \text{with } \sigma = 1, \dots, n$$

and we have spin-rapidity strings associated with them in the first *n* - 1 ranks: $k^{(n-1)} = \Lambda_m^{s(r)}$ for all ranks such that $n = r + m$.

We now incorporate the string solutions into the equations and simplify them using the notations and relations given in the second appendix. After some algebra, one arrives at the final version of the discrete-real-BAE:

$$e^{ink_j^{(n-1)} L} = \prod_{m=1} \prod_{i=1} e''_{nm} \left(k_j^{(n-1)} - k_i^{(m-1)} \right) \prod_{m=1} \prod_{\beta=1} e_m \left(k_j^{(n-1)} - \Lambda_{m\beta}^{s(n)} \right) \prod_{m=1} \prod_{\beta=1} e'_{nm} \left(k_j^{(n-1)} - \Lambda_{m\beta}^{q(1)} \right)$$

plus,

$$\prod_{m=1} \prod_{\beta=1} e_{nm} \left(\Lambda_{n\alpha}^{s(r)} - \Lambda_{m\beta}^{s(r)} \right) = \prod_{i=1} e_n \left(\Lambda_{n\alpha}^{s(r)} - k_i^{(r-1)} \right) \prod_{\sigma=\pm 1} \prod_{m=1} \prod_{\beta=1} e'_{nm} \left(\Lambda_{n\alpha}^{s(r)} - \Lambda_{m\beta}^{s(r+\sigma)} \right)$$

$$\prod_{m=1} \prod_{\beta=1} e_{nm} \left(\Lambda_{n\alpha}^{q(1)} - \Lambda_{m\beta}^{q(1)} \right) = \prod_{m=1} \prod_{i=1} e'_{nm} \left(\Lambda_{n\alpha}^{q(1)} - k_i^{(m-1)} \right) \prod_{m=1} \prod_{\beta=1} e'_{nm} \left(\Lambda_{n\alpha}^{q(1)} - \Lambda_{m\beta}^{q(2)} \right)$$

$$\prod_{m=1} \prod_{\beta=1} e_{nm} \left(\Lambda_{n\alpha}^{q(r)} - \Lambda_{m\beta}^{q(r)} \right) = \prod_{\sigma=\pm 1} \prod_{m=1} \prod_{\beta=1} e'_{nm} \left(\Lambda_{n\alpha}^{q(r)} - \Lambda_{m\beta}^{q(r+\sigma)} \right)$$

where we continue to use the notation $\Lambda_1^{q(M)} = \varepsilon$. The set of solutions of these equations determines the set of eigenvalues of the problem. Now all the unknowns are real valued variables.

1. Continuum Distributions Formulation

One can study the system in the *thermodynamic limit* where its size, *L*, and the number of electrons, *N_e*, both

tend to infinity with the density N_e/L being held fixed (one could later consider the *scaling limit*, when the density is allowed to go to infinity while some physical scale is kept fixed).⁴⁰ In that case the separation of distinct “solutions” is of order $O(1/N_e)$, so that rather than considering explicit “solutions” one can describe the system in terms of “densities of solutions”, typically to be denoted by $\rho(z)$, describing the number of solutions falling in a particular rapidity interval $(z, z + dz)$.⁷²

To determine the densities one proceeds by taking logarithms of the BAE obtaining transcendental equations for the rapidities characterized by integers that arise from the logarithmic branches. These integers label the “solutions” and are the quantum numbers of the eigenstate. One then constructs the *counting functions*⁴⁰ for the different rapidities [in our case $\nu_{cn}(z)$, $\nu_{sn}^{(r)}(z)$, and $\nu_{qn}^{(r)}(z)$]. The counting functions range over all integers: those that have been selected for a state correspond to “solutions”, or “roots”, and those integers that are omitted correspond to “holes”. We denote by ρ^r and ρ^h the various densities of roots and holes. For example $\rho_{qn}^{(r)}(z)$ denotes the density of roots of rank- r n -strings of quadrupolar rapidities. These density distributions are related to the counting functions:

$$\begin{aligned} L^{-1} \partial_z \nu_{cn}(z) &= \rho_{cn}(z) = \rho_{cn}^r(z) + \rho_{cn}^h(z) \\ L^{-1} \partial_z \nu_{sn}^{(r)}(z) &= \rho_{sn}^{(r)}(z) = \rho_{sn}^{r(r)}(z) + \rho_{sn}^{h(r)}(z) \\ L^{-1} \partial_z \nu_{qn}^{(r)}(z) &= \rho_{qn}^{(r)}(z) = \rho_{qn}^{r(r)}(z) + \rho_{qn}^{h(r)}(z) \end{aligned}$$

and should also obey the following relations,

$$\begin{cases} \frac{1}{L} N_{cn} = \int_k \rho_{cn}^r(k) \\ \frac{1}{L} M_{sn}^{(r)} = \int_\lambda \rho_{sn}^{r(r)}(\lambda) \\ \frac{1}{L} M_{qn}^{(r)} = \int_\lambda \rho_{qn}^{r(r)}(\lambda) \end{cases} .$$

These quantities are combined to define further ones,

$$\begin{cases} N_c = \sum_{n=1} n N_{cn} \\ M_s^{(r)} = \sum_{n=1} n M_{sn}^{(r)} \\ M_q^{(r)} = \sum_{n=1} n M_{qn}^{(r)} \end{cases}$$

where $N_c \equiv N_e$ corresponds to the number of electrons in the system. Further, the energy (that coincides with the momentum for a system with linear dispersion) and the number of particles with different spins or q -flavors are given by

$$\begin{cases} \frac{1}{L} E = \frac{1}{L} \varepsilon_q + \sum_{n=1} n \int_k k \rho_{cn}^r(k) \\ m_{sr} = M_s^{(r-1)} - M_s^{(r)} + \sum_{m=r} N_{cm} \\ m_{qr} = M_q^{(r-1)} - M_q^{(r)} + \delta_{r,1} N_c \end{cases}$$

where $r = 1, \dots, X$ for $SU(X)$ ($X = M, N$) and we remind the reader that $M_q^{(M)} = N_i = 1$ is the number of impurities in the system. Consistently with this convention we have the density $\rho_{q1}^{r(M)}(\lambda) = L^{-1} \delta(\lambda - \varepsilon)$. We will use these quantities to couple to crystal fields when we compute the thermodynamics.

Starting from the derivatives of the logarithm of the BAE and using the density distributions defined just above plus the convolution kernels defined in the second appendix one can write the continuum version of the BAE:

$$\begin{aligned} \rho_{cn}^h &= \frac{n}{2\pi} - C_{nm} * \rho_{cm}^r - K_m * \rho_{sm}^{r(n)} + B_{nm} * \rho_{qm}^{r(1)} \\ \rho_{sn}^{h(r)} &= -A_{nm} * \rho_{sm}^{r(r)} + K_n * \rho_{cr}^r + \\ &\quad + B_{nm} * \rho_{sm}^{r(r-1)} + B_{nm} * \rho_{sm}^{r(r+1)} \\ \rho_{qn}^{h(r)} &= -A_{nm} * \rho_{qm}^{r(r)} + \delta_{r,1} B_{nm} * \rho_{cm}^r + \\ &\quad + B_{nm} * \rho_{qm}^{r(r-1)} + B_{nm} * \rho_{qm}^{r(r+1)} \end{aligned}$$

(repeated indices are contracted). The way they are written, these equations determine the densities of holes as a function of the densities of roots and their solutions correspond to the different eigenvalues of the system.

A detailed analysis of these equations will be presented elsewhere. In the following we will use them as a starting point to write a second set of equations whose solution allows one to compute the free energy of the system and gives that way access to all thermodynamic quantities.

IV. THERMODYNAMIC BETHE-ANSATZ

The extension of the Bethe-Ansatz formalism to obtain finite temperature information was first done in the case of the Bose gas by C. N. and C. P. Yang.⁴¹ It was later adapted to the study of spin chains in the works of Gaudin,^{42,43} Takahashi,^{44,45} and others. The formalism is by now well developed and goes under the name of Thermodynamic Bethe-Ansatz (TBA). In the context of impurity models it was extensively used to find the impurity contributions to different thermodynamic quantities. In the following we outline the main steps and results of the TBA procedure as it applies to the multi-channel Anderson impurity model.

We shall proceed in a standard manner and derive an expression for the free energy of the system. We will work in the *grand canonical ensemble*, where the free energy is defined as⁷³

$$F = E - TS - \mu_c N_c - \sum_r h_{sr} m_{sr} - \sum_r h_{qr} m_{qr} .$$

Out of all the elements that enter this expression, the only one not mentioned in the previous section, and requiring special attention here, is the entropy. We define the entropy of a density distribution as follows (subindices are suppressed):

$$\frac{1}{L} \mathcal{S} \{ \rho^r, \rho^h \} = \rho^r \ln(1 + \eta) + \rho^h \ln(1 + \bar{\eta})$$

where we introduced the notational conventions $\eta = \rho^h/\rho^r$ and $\bar{\eta} = \eta^{-1} = \rho^r/\rho^h$. $\mathcal{S}\{\rho^r, \rho^h\}$ measures the number of microscopic states consistent with a given macroscopic (thermodynamic) state given by ρ^r and

ρ^h .⁴¹ For the sake of further compactness, we also introduce the notations $f = \ln(1 + \eta)$ and $\bar{f} = \ln(1 + \bar{\eta})$. We write down the explicit expression of a *free energy functional* for the system:

$$\begin{aligned} \frac{1}{L} \mathcal{F}\{\rho_x^{r,h}\} = & \frac{1}{L} \varepsilon_q + \frac{1}{L} h_{qM} + \sum_n \int_k \left[n(k - \mu_c - h_{q1}) - \sum_{i \leq n} h_{si} - T f_{cn} \right] \rho_{cn}^r - \sum_n \int_k T \bar{f}_{cn} \rho_{cn}^h + \\ & + \sum_{r,n} \int_\lambda \left[-(h_{sr+1} - h_{sr})n - T f_{sn}^{(r)} \right] \rho_{sn}^{r(r)} - \sum_{r,n} \int_\lambda T \bar{f}_{sn}^{(r)} \rho_{sn}^{h(r)} + \\ & + \sum_{r,n} \int_\lambda \left[-(h_{qr+1} - h_{qr})n - T f_{qn}^{(r)} \right] \rho_{qn}^{r(r)} - \sum_{r,n} \int_\lambda T \bar{f}_{qn}^{(r)} \rho_{qn}^{h(r)}. \end{aligned}$$

We next seek to determine the free energy, that in the thermodynamic limit we are allowed to evaluate as a saddle point: we vary \mathcal{F} with respect to the distributions ρ^r and ρ^h , subject to the constraint that they must satisfy the BAE. We thus obtain the so-called Thermodynamic Bethe-Ansatz equations:

$$\begin{aligned} f_{cn} = & n(k - \mu_c - h_{q1})/T - \delta_{n \geq i} h_{si}/T + \\ & + C_{nm} * \bar{f}_{cm} - K_m * \bar{f}_{sm}^{(n)} - B_{nm} * \bar{f}_{qm}^{(1)} \\ f_{sn}^{(r)} = & n(h_{sr} - h_{sr+1})/T + K_n * \bar{f}_{cr} + A_{nm}^{rs} * \bar{f}_{sm}^{(s)} \\ f_{qn}^{(r)} = & n(h_{qr} - h_{qr+1})/T - \delta_1^r B_{nm} * \bar{f}_{cm} + A_{nm}^{rs} * \bar{f}_{qm}^{(s)} \end{aligned}$$

(repeated indices are contracted and the kernels A_{nm}^{rs} are given in the second appendix). It is possible to reformulate the TBA equations as a set of recursions linking the different unknown distributions.⁴⁴ Such a formulation does not involve infinite sums and has also the virtue of rendering the structure of the problem more transparent. After a few algebraic manipulations – making extensive use of the recursion relations for the convolution kernels mentioned in the second appendix – one can re-express the TBA equations in what we call their *recursive formulation* (sometimes referred to as the Gaudin-Takahashi form). They read:⁷⁴

$$\left\{ \begin{array}{l} \text{Equations for the spin-rapidities:} \\ f_{sn}^{(r)} = \text{lex} \left(\delta_{n,1} G * \bar{f}_{cr} + G * f_{sn+1}^{(r)} + \hat{\delta}_{n,1} G * f_{sn-1}^{(r)} - G * \bar{f}_{sn}^{(r+1)} - G * \bar{f}_{sn}^{(r-1)} \right) \\ \\ \text{Equations for the flavor-rapidities:} \\ f_{qn}^{(r)} = \text{lex} \left(-\delta_{n \leq N} \delta_{r,1} G * \bar{f}_{cn} + G * f_{qn+1}^{(r)} + \hat{\delta}_{n,1} G * f_{qn-1}^{(r)} - G * \bar{f}_{qn}^{(r+1)} - G * \bar{f}_{qn}^{(r-1)} \right) \\ \\ \text{Equations for the charge-rapidities:} \\ \left\{ \begin{array}{l} \bar{f}_{cn < N} = \text{lex} \left(G * \bar{f}_{qn}^{(1)} + G * f_{s1}^{(n)} - G * f_{cn+1} - \hat{\delta}_{n,1} G * f_{cn-1} \right) \\ \text{plus the ‘driving’ equation,} \\ \left\{ \begin{array}{l} f_{cN} = \text{lex} \left(N \frac{\lambda}{\tau} - R G_t^{(M,M)} * f_{qN}^{(M-t)} + R G_m^{(N,M)} * \bar{f}_{cm} \right) \\ \bar{f}_{cN} = \text{lex} \left(-M \frac{\lambda}{\tau} - R G_m^{(N,N)} * \bar{f}_{cm} + R G_{t \leq M}^{(M,N)} * f_{qN}^{(M-t)} \right) \end{array} \right. \end{array} \right. \end{array} \right.$$

where the dimensionless variables $\lambda = \pi(k - \mu)/2\Delta$ and $\tau = \pi T/4\Delta$ were introduced⁷⁵ and, for convenience, we

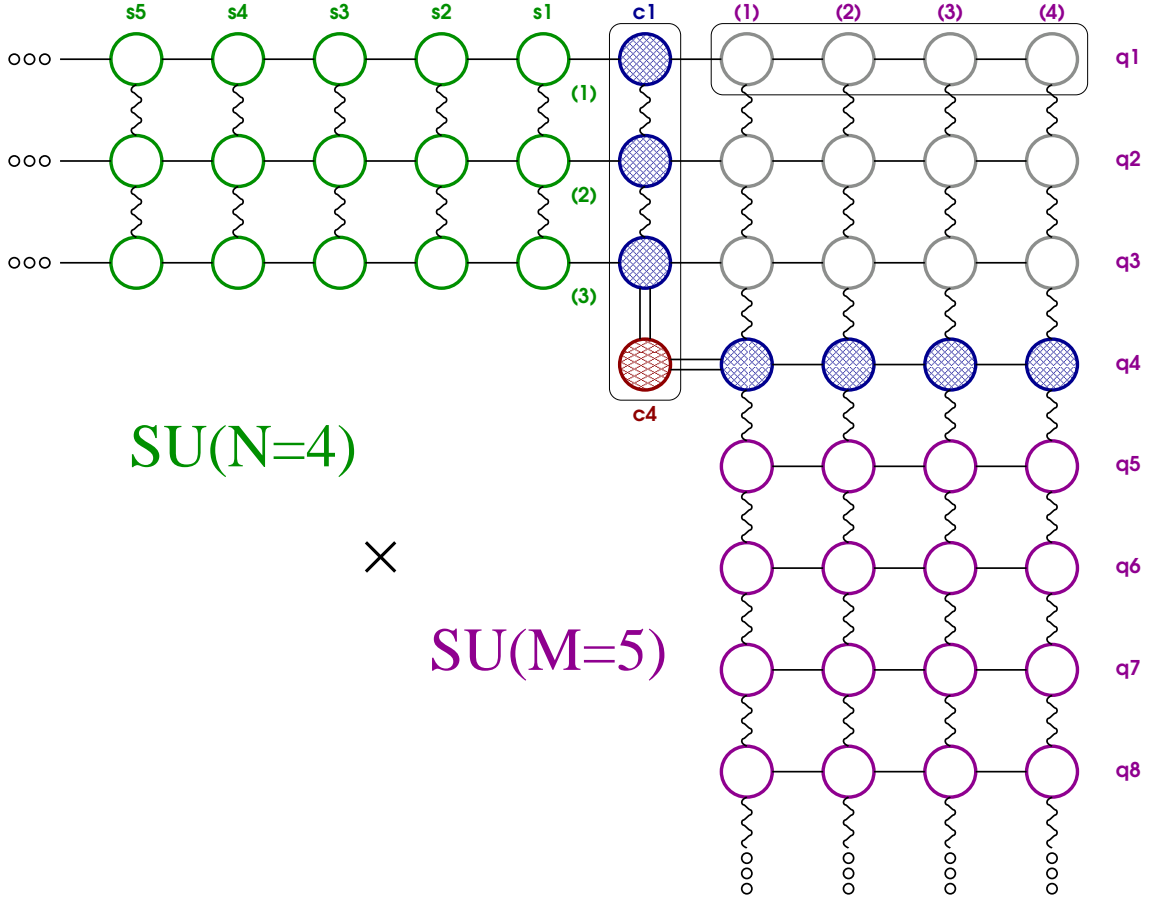


FIG. 3: TBA diagram for a particular realization of the multi-channel Anderson model in which the symmetry of the impurity is $SU(N) \otimes SU(M)$ with $N = 4$ and $M = 5$. A detailed explanation of this diagram is given in the text.

defined the function $\text{lex}(x) = \ln(1 + \exp(x))$. The general recursion kernels ($G_m^{(N,M)}$) and their regularized versions (${}^R G_m^{(N,M)}$) are discussed in the second appendix. The expressions for f_{cN} and \bar{f}_{cN} can of course be derived from each other, but here we write down both of them explicitly because both are useful in the numerical studies.

These equations are complemented by asymptotic conditions that are also a direct consequence of the ‘non-recursive’ TBA equations:

$$K_{n+1} * f_{xn}^{(r)} - K_n * f_{xn+1}^{(r)} \xrightarrow{n \rightarrow \infty} \alpha_x^r \equiv \frac{h_{xr+1} - h_{xr}}{T}$$

where h_{xr} is either $h_{sr=1,\dots,N}$ or $h_{qr=1,\dots,M}$ for the spin or quadrupolar f-distributions, respectively.

The structure of the recursive relations between the different distributions can be nicely visualized in a graph. In Fig. 3 we show an example of such a graph, a ‘TBA-diagram’ for a particular realization of the multi-channel Anderson model.

This representation of the equations highlights their connectivity and is the natural extension of the graphical representation commonly used in the case of other integrable models (for comparison and an example of

another related impurity model see the work on the multi-channel Coqblin-Schrieffer model⁴⁶). The different nodes correspond to the different distributions: (i) those in the horizontal stripe extending towards the left represent the $\eta_{sn}^{(r)}$, (ii) those in the vertical stripe extending downwards represent the $\bar{\eta}_{qn}^{(r)}$, and (iii) those in the vertical column enclosed in a box correspond to the $\bar{\eta}_{cN}$. The graph was drawn for the particular case of $SU(N=4) \otimes SU(M=5)$ symmetry, but its structure is generic. The horizontal straight lines indicate that the nodes are two-way connected by the equations according to $\ln \eta_{\text{node}} = G * T \ln(1 + \eta_{\text{neighbor}})$ and the vertical wavy lines indicate that the two-way connections are given by $\ln \eta_{\text{node}} = -G * T \ln(1 + \bar{\eta}_{\text{neighbor}})$. The double straight lines highlight the special kind of connections in the case of $\bar{\eta}_{cN}$.

There is a dual interpretation of this graph in terms of the reciprocals of all the distributions. Within this new picture the different nodes are as follows: (i) those in the horizontal stripe extending towards the left represent the $\bar{\eta}_{sn}^{(r)}$, (ii) those in the vertical stripe extending downwards represent the $\eta_{qn}^{(r)}$, and (iii) those in the vertical column enclosed in a box correspond to the

η_{cn} . The meaning of the straight and wavy lines also gets interchanged: horizontal straight lines now mean $\ln \eta_{\text{node}} = -G * T \ln(1 + \bar{\eta}_{\text{neighbor}})$ and vertical wavy lines mean $\ln \eta_{\text{node}} = G * T \ln(1 + \eta_{\text{neighbor}})$. This duality plays a role when one considers the two different integral valence limits, such limits will be discussed later.

The two boxes shown in the graph enclose those nodes that enter the expression for the impurity contribution to the free energy. Starting from the free energy functional and evaluating it using the distributions that obey the TBA equations, after a certain amount of algebra, one arrives at the expression $F = F_{\text{bulk}} + F_{\text{imp}}$ where

$$F_{\text{bulk}} = -\frac{L}{2\pi} \sum_n n \int_k T \ln(1 + \bar{\eta}_{cn})$$

and

$$F_{\text{imp}} = \varepsilon_q + \mu_q - \left[\sum_t G_t^{(M,M)} * T \ln(1 + \eta_{q1}^{(t)}) + \sum_m G_1^{(M+m,M)} * T \ln(1 + \bar{\eta}_{cm}) \right]_{k=\varepsilon}$$

from which all the different thermodynamic quantities of interest can be derived. Here F_{bulk} is the bulk contribution to the free energy (an extensive part that recovers the standard result for free electrons and is all there is in the absence of the impurity), on the other hand F_{imp} is the extra contribution due to the presence of the impurity. In the following we shall pursue the study of the latter.

As expected for an infinite flat-band, the bulk part of the free energy is found to be divergent. To study it, some form of regularization should be introduced, *e.g.* a bandwidth cut-off. A convenient procedure that was successfully applied in the Bethe-Ansatz study of the single-channel degenerate Anderson model is the introduction of a ‘Lorentzian cut-off scheme’,^{14,15,47} In that framework it is usual to fix the density and let the chemical potential be determined as an implicit function of the cut-off parameter. As a result the impurity thermodynamics is found to be naturally expressible in terms of a certain *scaling invariant* parameter, $\varepsilon^*(\varepsilon, \Delta)$,⁴⁸ an implicit function of cut-off, temperature, and fields.⁴⁷ On the other hand, the impurity contribution to the free energy is found to be regular (*i.e.* finite even in the limit of infinite cut-off). Since we shall be interested solely in the impurity thermodynamics, we will introduce no cut-off and continue to work always in the grand canonical ensemble, keeping fixed the chemical potential rather than the density. With this convention, we can continue to describe the physics in terms of the original microscopic parameter ε .

V. IMPURITY THERMODYNAMICS

In this section we study the impurity contributions to the different thermodynamic quantities of interest. We

will first list some analytical results and then give an extended discussion of the numerical solution of the TBA equations and the results obtained for several thermodynamic quantities across the different regimes of the model.

A. Analytical Results

As already pointed out in the two-channel case,²⁹ the multi-channel Anderson model displays a non-trivial zero temperature limit for the impurity contribution to the system entropy. This is a clear indication of the non-Fermi liquid character of the ground state. We can find the value of this entropy and identify the relevant scale for the cross-over into the low temperature phase in closed analytical form and for the general multi-channel case.

1. Zero Temperature Solution

We begin the study of the TBA equations by taking the zero temperature limit of the equations in order to identify the ground state. This is a required preliminary step before abording the study of the impurity contribution to the residual entropy.

It is convenient to introduce the distributions $\xi \equiv T \ln \eta$. Assuming that the derivatives $\partial_T \xi$ are bounded distributions, or have at most isolated logarithmic divergencies, we derive the following limits:⁴⁴

$$\begin{aligned} \lim_{T \rightarrow 0^+} T \ln(1 + \eta) &= |\xi| \quad \theta(\xi) \equiv \xi^+ \\ \lim_{T \rightarrow 0^+} T \ln(1 + \bar{\eta}) &= |\bar{\xi}| \quad \theta(\bar{\xi}) \equiv \bar{\xi}^+ = -\xi^- \end{aligned}$$

These limits are the key step in the derivation; using them it is immediate to write down the zero temperature limit of the equations,

$$\begin{aligned} NMz &= C_{Mt \leq M} * \xi_{qN}^{(M-t)+} - C_{Nm} * \bar{\xi}_{cm}^+ \\ \bar{\xi}_{cn < N} &= G * \left[\bar{\xi}_{qn}^{(1)+} + \xi_{s1}^{(n)+} - \xi_{cn+1}^+ - \hat{\delta}_{n,1} \xi_{cn-1}^+ \right] \\ \xi_{sn}^{(r)} &= \delta_{n,1} G * \bar{\xi}_{cr}^+ \\ &\quad + G * \left[\xi_{sn+1}^{(r)+} + \hat{\delta}_{n,1} \xi_{sn-1}^{(r)+} - \bar{\xi}_{sn}^{(r+1)+} - \bar{\xi}_{sn}^{(r-1)+} \right] \\ \xi_{qn}^{(r)} &= -\delta_{n \leq N} \delta_{r,1} G * \bar{\xi}_{cn}^+ \\ &\quad + G * \left[\xi_{qn+1}^{(r)+} + \hat{\delta}_{n,1} \xi_{qn-1}^{(r)+} - \bar{\xi}_{qn}^{(r+1)+} - \bar{\xi}_{qn}^{(r-1)+} \right] \end{aligned}$$

where the variable is the shifted rapidity $z = k - \mu$, and we use the notation $\hat{\delta}_{n,1} = 1 - \delta_{n,1}$. These equations can be solved exactly when $M = N$ and there are no external applied fields. Let us start discussing the two-channel case ($M = N = 2$). Since there is only one rank we drop the rank superindex during this discussion. It is easy to see from the equations that $\xi_{sn}^- = 0 \forall n$ and $\bar{\xi}_{qn}^- = 0 \forall n > 2$. It is natural to assume in the

zero fields case that $\xi_{c1}^- = 0$, which implies $\xi_{q1}^- = 0$. Notice that after these considerations the equations for the spin rapidities are decoupled from the rest. We solve them first, taking into account the asymptotic condition $K_{n+1} * \xi_{sn} - K_n * \xi_{sn+1} \rightarrow -2h_s = 0$ (we use the standard definition for the magnetic field). The solution is very simple: put all ξ_{sn} 's to zero. We see also that in analogy to the spin case we can solve for the q-flavor sector simply by taking all ξ_{qn}^+ 's with $n \neq 2$ to be zero. Only three non-zero distributions remain and are given directly by the equations

$$\begin{cases} \xi_{c2} = \xi_{c2}^+ + \xi_{c2}^- = 2z \\ \begin{cases} \xi_{c1} = \xi_{c1}^+ = G * \xi_{c2}^+ \\ \xi_{q2} = \xi_{q2}^- = G * \xi_{c2}^- \end{cases} \end{cases}$$

Thus, in the absence of external fields, the ground state is built out of a sea of charge-spin strings filled up to the chemical potential (*i.e.* $k = \mu$) and a completely filled sea of q-flavor 2-strings. We can derive the zero temperature impurity valence, or level occupancy, in a closed form (we use the notations $\lambda = \pi z / 2\Delta$ and $J = 2\Delta / (\varepsilon - \mu)$, notice the charge susceptibility can be easily obtained taking a derivative):

$$n_{c,\text{imp}}^0 = \int_{-\infty}^{+\infty} \frac{4(\lambda - \pi/J)}{[(\lambda - \pi/J)^2 + \pi^2]^2} \xi_{q2}(\lambda) d\lambda.$$

The occupancy is integral (*i.e.* $n_c^0 \approx 0, 1$) for $|\varepsilon - \mu| \gg \Delta$, and non-integral otherwise. It is a simple exercise to show that the impurity contribution to the residual entropy is $S_{\text{imp}}^0 = \ln \sqrt{2}$ – a result that is consistent with what was found in the integral valence limit given by the two-channel Kondo model.¹⁶ We will give below a derivation of S_{imp}^0 for the general multi-channel case.

Let us now return to the case with arbitrary values of M and N , but always in the absence of applied external fields. The equations are more involved and one is not able to make general statements about the positivity of the different distributions the way we did in the two-channel case. We proceed by making the following educated guess:

1. $\xi_{sn}^{(r)} = 0 \quad \forall n, r$ (this is to ensure a paramagnetic ground state), and it implies $\bar{\xi}_{cr < N}^+ = 0$.
2. $\xi_{qn}^{(r)} = 0 \quad \forall n \neq N$ and for $n = N$ the distributions are negative, *i.e.* $\xi_{qN}^{(r)+} = 0$.

The equations then take the form,

$$\begin{aligned} NMz &= C_{MM} * \xi_{cN}^+ - C_{NN} * \bar{\xi}_{cN}^+ \\ \xi_{cn < N}^+ &= G * [\xi_{cn+1}^+ + \hat{\delta}_{n,1} \xi_{cn-1}^+] \\ \bar{\xi}_{qN}^{(r)+} &= \delta_{r,1} G * \bar{\xi}_{cN}^+ + G * [\bar{\xi}_{qN}^{(r+1)+} + \bar{\xi}_{qN}^{(r-1)+}] \end{aligned}$$

The first equation is decoupled from the rest and one should solve it to determine ξ_{cN} that will later play the role of a driving term on the other equations. A solution that is exact when $N = M$, but approximate otherwise, is given by $\xi_{cN} = z [M \theta(-z) + N \theta(z)]$. When approximate, this solution is not accurate in the rapidity interval $|z| < \Delta$. This region corresponds, in the free energy, to the mixed valence regime that interpolates between two different multi-channel Coqblin-Schrieffer limits (this will be discussed more in detail in Secs. V A 3 and VI). When $N \neq M$, the above solution can be used as the initial guess for an iterative numerical scheme; this idea will also be useful for the numerical solution of the finite temperature case. The remaining two sets of equations can then be ‘unnested’ to obtain explicit expressions for the different remaining distributions, all of which are fully determined by ξ_{cN} (in complete analogy to the two-channel case).

2. Residual Impurity Entropy

Regardless of its precise form, the solution for ξ_{cN} will have both positive and negative non-zero parts (as is clear from considering the large $|z|$ asymptotic limits). Thus, the zero temperature and fields solution discussed earlier indicates that $\xi_{cn < N}^+$ and $\bar{\xi}_{qN}^{(r)+}$ are non-zero everywhere.⁷⁶ In turn this means that $\bar{\eta}_{cn < N}$ and $\eta_{qN}^{(r)}$ are zero in the zero temperature limit. At the level of the TBA equations, this has the effect of isolating the equations for the $\eta_{qn < N}^{(r)}$ distributions:

$$\begin{aligned} \ln \eta_{qn < N}^{(r)} &= G * [\hat{\delta}_{n,N-1} \ln(1 + \eta_{qn+1}^{(r)}) + \\ &\quad + \hat{\delta}_{n,1} \ln(1 + \eta_{qn-1}^{(r)}) - \\ &\quad - \ln(1 + \bar{\eta}_{qn}^{(r+1)}) - \ln(1 + \bar{\eta}_{qn}^{(r-1)})] \end{aligned}$$

The reader should notice our earlier result, that the related distributions $\xi_{qn < N}^{(r)}$ are all zero at zero temperature, merely indicates that the respective $\eta_{qn < N}^{(r)}$ are finite (*i.e.* neither zero nor divergent). The equations above contain no driving terms, therefore the distributions should be constant functions of z . In such a case we can make the replacement $G \rightarrow \delta(z)/2$ and performing the convolutions obtain a purely algebraic set of equations,

$$\left(\eta_{qn < N}^{(r)}\right)^2 = \frac{(1 + \eta_{qn+1}^{(r)})(1 + \eta_{qn-1}^{(r)})}{(1 + \bar{\eta}_{qn}^{(r+1)})(1 + \bar{\eta}_{qn}^{(r-1)})}$$

that, is easy to verify, admits the solution

$$\eta_{qn}^{(r)} = \frac{\sin\left(\frac{n+r}{N+M}\pi\right) \sin\left(\frac{n+M-r}{N+M}\pi\right)}{\sin\left(\frac{r}{N+M}\pi\right) \sin\left(\frac{M-r}{N+M}\pi\right)} - 1.$$

Plugging this result in the expression for the free energy we read off the residual impurity entropy:

$$S_{\text{imp}}^0 = \ln \frac{\sin \frac{\pi M}{N+M}}{\sin \frac{\pi}{N+M}} = \ln \frac{\sin \frac{\pi N}{N+M}}{\sin \frac{\pi}{N+M}}.$$

This formula agrees with the one that was derived in the integral valence limit⁴⁶ using the multi-channel version of the Coqblin-Schrieffer model.^{49,50} That model is the Schrieffer-Wolff limit⁵¹ of the multi-channel Anderson model that we are studying. We now turn to the discussion of such limit.

3. Integral Valence or Schrieffer-Wolff Limit

In the standard approach – at the level of the Hamiltonian – the Schrieffer-Wolff (SW) limit is defined as a truncated unitary transformation that eliminates the direct hybridization term and traces over (discards) the less favorable states of valence from the impurity Hilbert space. This limit leads to a projection onto a Hilbert subspace with the impurity site permanently occupied by a *local moment*. Starting from H_{MchA} , one obtains this way the multi-channel Coqblin-Schrieffer (CS) model (the N -channel $SU(M)$ model or the M -channel $SU(N)$ one depending on the sign of ε , see below). In the following we will discuss how this effective limiting procedure can be carried out at the level of the TBA equations.

Let us point out that the SW-transformation can be viewed as a first step in a more detailed Renormalization Group analysis (which we will not carry out in here). The multi-channel CS-model is therefore, when away from mixed valence, the *naïve* low temperature effective Hamiltonian of the full multi-channel Anderson model. This effective Hamiltonian is relevant for the description of the low energy dynamics for energy scales $E \ll T_H$. In other words,

$$H_{\text{MchA}} \rightarrow H_{\text{CS},x} + \left[\mathcal{O}\left(\frac{E}{T_H}\right) \text{ corrections in all sectors} \right]$$

(with $x = s, q$ for the magnetic or quadrupolar sector, respectively). In the limit of $|\varepsilon| \rightarrow +\infty$, $T_H \rightarrow +\infty$ and the projection is exact (albeit with a vanishing exchange constant). For any finite T_H , the effects of the corrections, though ‘subleading’ to those kept in $H_{\text{CS},x}$, may be important at low enough temperatures if they combine with other operators to provide more singular contributions. This will be the case, for instance, when the degeneracy of the lower-energy impurity configuration exceeds that of the (degenerate) higher-energy one, as we shall stress in Sec. VI. We conclude therefore that the SW-transformation needs to be used with extreme care in circumstances like the one described above.

We now turn to studying the integral valence limit via the Bethe-Ansatz. The discussion of the integral valence limit turns out to be simpler using an ‘inverted’ set of TBA equations (trading back the recursions on the rank

indices for finite sums). In this alternative formulation, the equations read (see the appendix for the kernel definitions),

$$\begin{aligned} -\bar{f}_{sn}^{(r)} &= R_N^{rs} * \left[f_{sn+1}^{(s)} + \hat{\delta}_{n,1} f_{sn-1}^{(s)} + \delta_{n,1} \bar{f}_{cr} - G^{-1} * f_{sn}^{(s)} \right] \\ -\bar{f}_{qn}^{(r)} &= -\delta_{n,N} \tau^{-1} \Delta E_q^r + \\ &\quad + R_M^{rs} * \left[f_{qn+1}^{(s)} + \hat{\delta}_{n,1} f_{qn-1}^{(s)} - G^{-1} * f_{qn}^{(s)} - \delta_{n < N} \delta_{s,1} \bar{f}_{cn} \right] \\ -f_{cn < N} &= -\tau^{-1} \Delta E_s^n + \\ &\quad + R_N^{nm} * \left[\bar{f}_{qm}^{(1)} + f_{s1}^{(m)} - G^{-1} * \bar{f}_{cm < N} \right] \end{aligned}$$

where we defined the effective *driving terms* (we remind the reader that $\tau = \pi T / 4\Delta$),

$$\begin{aligned} \Delta E_q^r / \tau &\equiv R_M^{r1} * \bar{f}_{cN} \\ \Delta E_s^n / \tau &\equiv R_N^{nN-1} * f_{cN}. \end{aligned}$$

We need to discuss separately the quadrupolar and the magnetic scenarios. The calculations are very similar in both cases. We turn our attention to the former. In the quadrupolar SW limit ($\varepsilon_q \ll \varepsilon_s$),⁷⁷ the $SU(N) \otimes SU(M)$ Anderson model maps into an N -channel CS-model for a local $SU(M)$ quadrupolar impurity. The key to understand this limit is the study of the driving terms.

At low temperatures – in a sense that will become precise below – and for $|\lambda| \gg 1$ (*i.e.* away from the intrinsic mixed-valence region) we can make the following approximation – motivated by our zero temperature solution for the ground state – that captures the leading functional dependence in temperature and rapidity of the distribution associated to the maximal charge-spin bound states: $f_{cN} \simeq \text{lex}(M\lambda/\tau) \theta(-\lambda) + \text{lex}(N\lambda/\tau) \theta(\lambda)$. The effective driving terms can then be approximated as (for $\lambda \gg 1$ in the quadrupolar case),

$$\begin{aligned} \Delta E_q^r &\simeq -R_M^{r1} * [M\lambda]^- \xrightarrow{\lambda \gg 1} \frac{M^2}{4\pi} \sin \frac{\pi(M-r)}{M} e^{-\frac{2}{M}\lambda} \\ \Delta E_s^n &\simeq R_N^{nN-1} * [N\lambda]^+ \xrightarrow{\lambda \gg 1} n\lambda. \end{aligned}$$

As the temperature is lowered, both driving terms diverge. But since we have that $\Delta E_s^n \gg \Delta E_q^r$ due to the different dependence in rapidity, $\Delta E_s^n / \tau$ will drive to zero the distributions for the charge rapidities ($f_{cn < N}$) faster than $\Delta E_q^r / \tau$ will drive the $f_{qn}^{(r)}$ ’s. That way the $f_{qn}^{(r)}$ ’s are effectively cut away from the other distributions (in this case the $f_{sn}^{(r)}$ ’s) and they alone determine the impurity thermodynamics. The free energy is given by

$$F_{\text{imp}} / \tau \simeq \varepsilon_q + \mu_q - \frac{1}{2\pi} \sum_t \int \frac{\sin \frac{\pi t}{M}}{\cos \frac{\pi t}{M} + \cosh \xi} f_{q1}^{(t)}(\xi) d\xi$$

where we performed the change of variables $M\xi = 2\pi/J - 2\lambda$ and redefined the $f_{q1}^{(t)}$ ’s as functions of the new variable ξ . The goal of this change of variables is to

remove the *coupling constant* (J) dependence from the expression of the free energy and move it into the TBA equations. The only explicit dependence on J will be in the driving terms and the same is true for the explicit temperature dependence; this fact will allow us to identify the natural temperature scales of the system. Remark that, in terms of the new variables, the main contribution to the free energy comes from the value of the distributions around $\xi \approx 0$.

a. High Temperature Scale: Consider the driving terms ΔE_s^n . Changing variables we obtain,

$$\Delta E_s^n / \tau \xrightarrow{\lambda \gg 1} n\lambda / \tau = \left(\frac{n\pi}{J} - \frac{nM}{2}\xi \right) / \tau \approx \left(\frac{n\pi}{J} \right) / \tau .$$

We shall thus define the Schottky temperature scale (the name will find its motivation later, with the discussion of the specific heat):

$$\tau_S \equiv \frac{N\pi}{2J} \implies T_S = \frac{N\Delta}{J} .$$

For $\tau < \tau_S$ (and $J < 1$), the valence fluctuations are quenched and the model goes into a regime where an effective description in terms of a CS-model becomes appropriate. The distributions associated to the charge rapidities go to zero and isolate the ones associated to the quadrupolar rapidities that form a system of TBA equations identical to the one of the CS-model. Notice that, as the temperature is lowered, these driving terms diverge faster than the other ones that have to overcome a decaying exponential in the numerator (cf. with the caveats about the SW-transformation discussed above).

b. Low Temperature Scale: Consider now the driving terms ΔE_q^r . Changing variables once more we obtain

$$\Delta E_q^r / \tau \xrightarrow{\lambda \gg 1} \frac{2}{N} \sin \frac{\pi(M-r)}{M} e^{\xi - \ln(\tau/\tau_K)}$$

where

$$\tau_K \equiv \frac{NM^2}{8\pi} e^{-\frac{2\pi}{MJ}} \implies T_K = N\Delta \left(\frac{M}{2\pi} \right)^2 e^{-\frac{2\pi}{MJ}} .$$

We have chosen to leave a factor of $2/N$ outside of the definition of the Kondo scale in order to have a complete resemblance between the resulting TBA equations and those for the scaling limit of a multi-channel CS-model⁴⁶ (that CS-model, together with a cut-off prescription $D_{\text{eff}} = NM^2\Delta/4\pi^2$, is therefore the appropriate low energy effective theory). Since the equations match, all the analysis done for that model (finding the leading exponents of the specific heat coefficient and susceptibilities, etc.) applies in this limit and we do not need to repeat those considerations here.⁴⁶

c. The two Scales: For the *magnetic moment limit* ($\varepsilon_s \ll \varepsilon_q$) we would find again two scales with the roles of M and N interchanged (we omit the details since the considerations are very similar). As a shorthand, we can extrapolate the two low energy scales (quadrupolar and magnetic) into the high energy scales of the other regime (for the opposite sign of ε). This serves the extra purpose of providing an *ad hoc* interpolation between both regimes and across the intrinsic mixed valence region. We can define thus the two scales,⁷⁸

$$T_q \equiv \frac{2\Delta}{\pi} \tau_q \approx \frac{2\Delta}{\pi} (M/2)^2 \ln \left(1 + \frac{N}{2\pi} e^{-\frac{2\pi}{MJ}} \right)$$

$$T_s \equiv \frac{2\Delta}{\pi} \tau_s \approx \frac{2\Delta}{\pi} (N/2)^2 \ln \left(1 + \frac{M}{2\pi} e^{\frac{2\pi}{NJ}} \right) .$$

The role of these two temperature scales was illustrated in the schematic picture of Fig. 2. In terms of them we can further write,

$$T_H(\varepsilon) \equiv \max \{T_s(\varepsilon), T_q(\varepsilon)\} \xrightarrow{|\varepsilon| \gg \Delta} T_S(\varepsilon)$$

$$T_L(\varepsilon) \equiv \min \{T_s(\varepsilon), T_q(\varepsilon)\} \xrightarrow{|\varepsilon| \gg \Delta} T_K(\varepsilon)$$

that serve as boundaries among the high-, intermediate-, and low-temperature regimes. At high temperatures the impurity is in a mixed valence state. As the temperature is lowered, the system crosses the first temperature scale indicated as T_H , for $|\varepsilon| \gtrsim \Delta$ this coincides with T_S (the chemical potential is taken to be zero to lighten the notation). At this point the system enters a regime that can be approximately described with the respective CS-model. At first, the system is in the ‘unscreened’ local moment regime, extending between T_H and the lower scale $T_L = T_K$. The larger the value of $|\varepsilon|$ the wider the temperature window of this regime. For $|\varepsilon| \lesssim \Delta$ the two energy scales merge, indicating that there is no moment formation. As the temperature is lowered beyond T_L , the moment screening commences and the physics is asymptotically governed by a line of fixed points parametrized by the value of ε/Δ (or some observable that depends on it and varies along the line, as for instance the charge valence of the impurity). The different points in the line share the same value for the impurity entropy, and the same set of leading exponents of the specific heat coefficient (*i.e.* $\gamma = C_{\text{imp}}/T$) or the different susceptibilities. However, the prefactors of the different leading terms will in general vary along the line and could in principle be determined by direct measurement. Thus a multi-channel Kondo effect takes place for any ε as the temperature is lowered. It is amusing to note that for $\varepsilon = 0$, in particular, the Kondo effect takes place *without* moment formation.

4. Asymptotic values

In this section we will be interested in finding the values that the different distributions (in this case the η 's) take when $\lambda \rightarrow \pm\infty$. This corresponds to the limit of infinite $|\varepsilon - \mu|$ at *finite temperature*. These results will be required in the next section, where the numerical solution of the TBA equations is discussed. Remark that, due to the behavior of the two energy scales derived above, in the limits considered in this section one always has $T_k \lll T \lll T_s$ and the $\lambda \rightarrow \pm\infty$ limits shall be, respectively, identified with the *infinite* temperature limits of the effective quadrupolar and magnetic multi-channel CS-models.

From the results above and inspection of the equations, the reader can convince himself that,

$$\left\{ \begin{array}{l} \left\{ \begin{array}{l} \lim_{\lambda \rightarrow +\infty} f_{cN} = +\infty \\ \lim_{\lambda \rightarrow +\infty} \bar{f}_{cN} = 0 \end{array} \right. \\ \left\{ \begin{array}{l} \lim_{\lambda \rightarrow -\infty} f_{cN} = 0 \\ \lim_{\lambda \rightarrow -\infty} \bar{f}_{cN} = +\infty \end{array} \right. \end{array} \right.$$

We shall use this result to analyze the TBA equations in the asymptotic limit. The two limits, $\lambda \rightarrow \pm\infty$, are different and we shall consider them separately.

a. Right Asymptotics: Let us first study the limit of $\lambda \rightarrow +\infty$ that we call the right asymptotics of the distributions. We want to find the values $\bar{\eta}_{xn}^{(r)} = \lim_{\lambda \rightarrow +\infty} \eta_{xn}^{(r)}$ that the different distributions take in the limit (with $x = s, q$). Except for η_{cN} that is unbounded, all the other η 's acquire finite values and for λ very large can be taken as constants. From the limit $f_{cN} \xrightarrow{\lambda \rightarrow +\infty} +\infty$ it follows that all the $\bar{\eta}_{cn < N}$'s go to zero and the equations for the $\bar{\eta}_{sn}^{(r)}$'s and those for the $\bar{\eta}_{qn}^{(r)}$'s form two identical sets decoupled from each other and obeying the following recurrence relation:

$$\bar{\eta}_{xn+1}^{(r)} + 1 = \left(1 + \frac{\bar{\eta}_{xn}^{(r+1)}}{\bar{\eta}_{xn}^{(r)}} \right) \frac{\left(\bar{\eta}_{xn}^{(r)} \right)^2}{\left(1 + \frac{\bar{\eta}_{xn-1}^{(r)}}{\bar{\eta}_{xn}^{(r)}} \right)} \left(1 + \frac{\bar{\eta}_{xn}^{(r-1)}}{\bar{\eta}_{xn}^{(r)}} \right).$$

In the case of uniform or 'Zeeman' splitting, all the α_x^r 's entering the large n asymptotic condition are equal and an analytic solution for the asymptotic values is known. It is easy to show with some algebra that the solutions are:^{16,46,52,53}

$$\bar{\eta}_{xn}^{(r)} + 1 = \frac{\sinh((n+r)\alpha_x) \sinh((n+N_x-r)\alpha_x)}{\sinh(r\alpha_x) \sinh((N_x-r)\alpha_x)} \xrightarrow{\alpha_x \rightarrow 0} \frac{(n+r)(n+N_x-r)}{r(N_x-r)}$$

where $N_s = N$, $N_q = M$ and α_x lost its dependence on the rank index. A closed analytic solution is not known for the case of a more general *crystal field splitting* (more general splittings might be relevant to make the connection with the experimental systems that motivated the model, this point will be discussed further in the next section). Notice that when the values of the $\bar{\eta}$'s are required for a particular splitting, they can always be found numerically.

b. Left Asymptotics: We study now the opposite limit of $\lambda \rightarrow -\infty$, in order to find the asymptotic values $\bar{\eta}_{xn}^{(r)} = \lim_{\lambda \rightarrow -\infty} \eta_{xn}^{(r)}$. Except for $\bar{\eta}_{cN}$ that is unbounded, all the other η 's acquire finite values and for λ very large can be taken as constants. From the limit $\bar{f}_{cN} \xrightarrow{\lambda \rightarrow -\infty} +\infty$ it

follows that all the $\bar{\eta}_{qn}^{(r)}$'s go to zero and the equations for the remaining distributions form two identical sets decoupled from each other and similar to those of the right asymptotic limit. The solution of that case can be applied to this one if the following identifications are made (cf. with the discussion of Fig. 3):

$$\left\{ \begin{array}{l} \bar{\eta}_{sn}^{(r)} = \bar{\eta}_{sM+n}^{(r)} \\ \bar{\eta}_{cn < N}^{(r)} = \bar{\eta}_{sM}^{(n)} \\ \bar{\eta}_{qn < N}^{(r)} = \bar{\eta}_{sM-r}^{(n)} \\ \bar{\eta}_{qN}^{(r)} = 0 \\ \bar{\eta}_{qn > N}^{(r)} = \bar{\eta}_{qn-N}^{(r)} \end{array} \right.$$

These are the same identifications that would be required for an explicit discussion of the Schrieffer-Wolff limit in the local magnetic moment regime, ($\varepsilon_s \ll \varepsilon_q$), in order to match the resulting TBA equations to those of the corresponding magnetic multi-channel CS-model.

Once the right and left asymptotic limits are both known, one is then ready to tackle the problem of solving the TBA equations numerically; as we proceed to explain in the latter parts of this section.

B. Numerical Solution

In order to access the thermodynamics of the system at all temperatures, we shall resort to the numerical solution of the TBA equations. This task was carried out in the past for other integrable impurity models.^{46,54,55,56,57} The equations of the multi-channel Anderson impurity model have many similarities with those considered previously for other types of impurities, but they present also important differences. We give below a brief outline of the numerical procedure that we developed followed by the results we thus obtained.

1. Outline of the Numerical Procedure

We solve the TBA equations using a standard iterative scheme first introduced in the work of Rajan.⁵⁴ The idea is to use the TBA equations in their recursive formulation, start with some educated initial guess, and iterate them until certain convergence criterion is met (this general scheme is sometimes known as Kepler's method; cf. Ref. [58]). Our particular implementation borrows ideas mainly from the previous work by Costi and Zarád for the anisotropic Kondo model.⁵⁶ In that work, the closure of the infinite set of TBA equations into a finite set brings in a great simplification. This is not, however, the case in general and we need to address the issue of truncation of the infinite hierarchy of recursions. The standard procedure is to define some boundary levels (in our case $f_{sn_s+1}^{(r)}$ and $f_{qn_q+1}^{(r)}$, for suitably large values n_s and n_q of the level index) and fix them. It was done in the past by taking those boundary distributions as constants equal to the average of their right and left asymptotic values that are known analytically.^{54,58} This approximation is good when n_s and n_q are fairly large (depending on the particular model). In the case at hand the TBA equations are more complicated than those for the Kondo model (in a way that will become clear below) and we cannot afford the computational cost of taking too large values for n_s and n_q . The alternative we found was to start with some educated guess for the distributions up to $f_{xn_x+1}^{(r)}$ (with $x = s, q$) that interpolates smoothly between the right and left asymptotic values (discussed above) respecting the monotonicity properties of the solution. Then we iterate the equations to find new values for the different distributions up to the levels $n = n_s, n_q$. At the end of each iteration we update the value of the boundary distributions ($n = n_s + 1, n_q + 1$) using the $f_{xn_x}^{(r)}$'s suitably shifted and rescaled to match the analytically known asymptotic values corresponding to the boundary levels. This procedure is repeated until stable convergence is achieved on the free energy function that we recalculate at each iteration.

The rapidity dependence of the distributions in the case of the Kondo TBA equations is associated to variations in temperature, and the two asymptotic limits correspond to the zero and infinite temperature limits.³⁴ This is in contradistinction to the case of the TBA equations for the multi-channel Anderson model, for which the rapidity dependence is related to variations of the coupling ($\sim 1/J$). We will therefore require modest computational effort to compute the free energy for different values of the coupling and determine quantities like charge susceptibilities, but temperature dependence will require independent runs for each value of temperature required. Since determining temperature dependence is essential, our computational task becomes typically two to three orders of magnitude larger than for Kondo impurities; depending on the range and number of temperature points desired and not counting the inherent extra complexity of our TBA equations.

Once we have a finite number of equations involving a finite number of continuous distributions, we need to discretize those distributions. This is conceptually done in two steps, the first one being the introduction of cut-offs on the rapidity axis. We have to choose large right and left cut-offs that enter once the distributions are approximately constant functions of the rapidity reaching their respective right and left asymptotic values. Second, we need to discretize the axis interval between the cut-offs. This is done defining three regions. First a small region centered around zero that we discretize using a fine mesh. The size of this region is chosen depending on the parameters of the problem so that it encloses all the intervals where different distributions show rapid variations. This typically happens for region boundary values of the rapidities such that the magnitude of their associated coupling corresponds to a Kondo temperature of the order of the temperature set for the system. Second, the two regions to the right and left of the central one are discretized logarithmically until reaching the cut-offs defined above. In these shoulder regions all the distributions vary slowly as they attain their asymptotic values.

The different convolution kernels required in the calculations should be evaluated, this is done a single time at the beginning of the calculations when they are stored as matrices. The kernels are relatively rapidly varying functions of the rapidities as compared with the TBA distributions, so we discretize them using a denser mesh. We use a mesh that is locally n times (typically $n \sim 10$) finer than the one used for the TBA distributions and these are interpolated to the points in the finer mesh using cubic splines. The extra points in the finer mesh are chosen to be the n -th order quadrature points of each subinterval of the coarser one. The convolution integrals can thus be split into the different subintervals and carried out with high precision in each one of them using Gaussian quadrature (corrections for the introduction of the right and left cut-offs are also implemented). Since accuracy is very important for certain applications,³⁰ the evaluation of the different kernels requires a high precision implementation of the sums involving four digamma functions of complex arguments (see appendix). To carry it out we wrote an algorithm based on 'a precision approximation of the gamma function' due to Lanczos.⁵⁹

With everything set to start the iterative evaluation of the TBA equations, one last point is worth mentioning. The evaluation of the right-hand side of these equations requires the implementation of the ubiquitous function $\text{lex}(x)$. This implementation is, however, unsurprisingly subtle. We first notice that, since $\text{lex}(x) = [x]^+ + \text{lex}(-|x|)$, it suffices to implement the function for negative arguments. This we do by first evaluating $e^{-|x|}$ and then using a careful implementation of $\ln(1+x)$ with the property of cancellation of rounding errors.⁶⁰ This algorithm ensures monotonicity, machine precision accuracy, and 'graceful underflow'.

We show below some of the results that were obtained with different implementations of the described numeri-

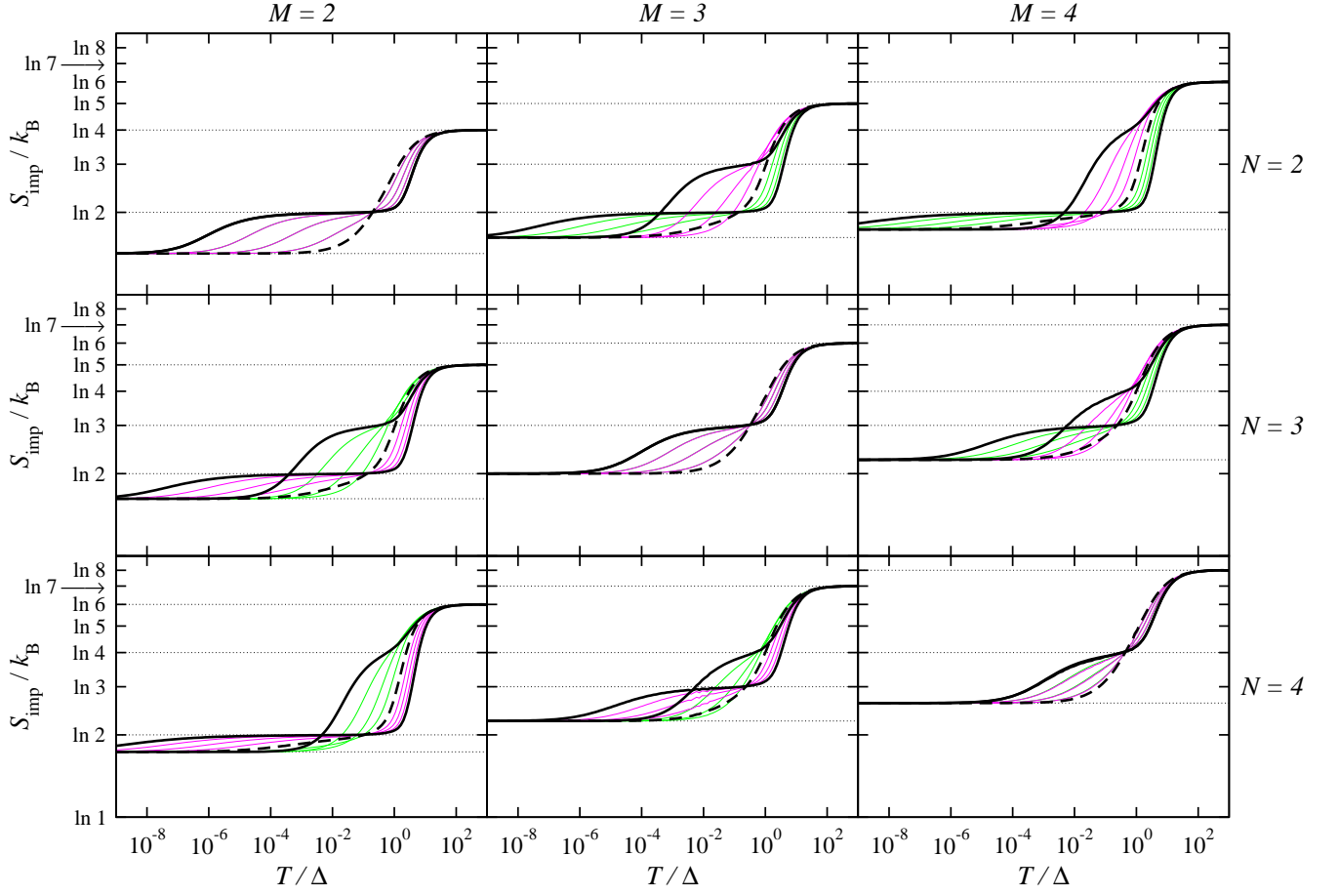


FIG. 4: Impurity entropy as a function of temperature. The different curves correspond to: $\varepsilon/\Delta = 0$ (dashed lines); $\varepsilon/\Delta = \pm 2, \pm 4, \pm 6$ (light lines); and $\varepsilon/\Delta = \pm 8$ (dark solid lines). The different panels give the results for different values of N and M as indicated to the right and above, respectively. Curves for different signs of ε are degenerate in the diagonal panels. In the off-diagonal ones they can be identified from the value of the entropy in the intermediate plateaux (see text).

cal procedure.

2. Numerical Results

As stated above, one of the important issues that makes the numerical analysis of the TBA equations required is the study of the temperature dependence in its full range. We give below illustrative results of this dependence where the presence of the two cross-over scales discussed already on analytic grounds is clearly observed. We start by showing results for the model in the absence of crystalline or external applied fields.

In Fig. 4 we show several plots of the entropy as a function of temperature. The different panels correspond to different symmetries of the model; $N = 2, 3, 4$ row-wise and $M = 2, 3, 4$ column-wise as indicated. The different curves in each panel correspond to different values of the energy splitting between the two impurity configurations ($\varepsilon = \varepsilon_s - \varepsilon_q$) and, without loss of generality, the total chemical potential is taken to be zero.⁷⁹ In all the pan-

els, the dark solid lines correspond to $\varepsilon/\Delta = \pm 8$ and the dark dashed line corresponds to the *extreme* mixed valence case of $\varepsilon = 0$ (or $\varepsilon = \mu$). The remaining thin lines correspond to intermediate values of the energy splitting ($\varepsilon/\Delta = \pm 2, \pm 4, \pm 6$) and are given to illustrate how the system *interpolates* among the different limits of large, positive and negative, and vanishing ε . On the one hand, in the high-temperature limit, the entropy is in each case given by $S_{\text{imp}}^{\infty}(N, M) = k_B \ln(N + M)$; as expected since $N + M$ is the total size of the impurity Hilbert space. On the other hand, in the low-temperature limit, the value of the entropy tends to the $S_{\text{imp}}^0(N, M)$ values we found analytically (see Sec. V A 2). We remark that both these limiting values are independent of ε .

For intermediate temperatures, the figure shows how the impurity entropy is quenched from its high- to its low-temperature values as the temperature decreases. This happens as a two stage process for large values of ε (solid lines) and as a single stage process in the mixed valence case (dashed lines), all in accordance with the theoretical discussion given above (see Fig. 2 and the discussion

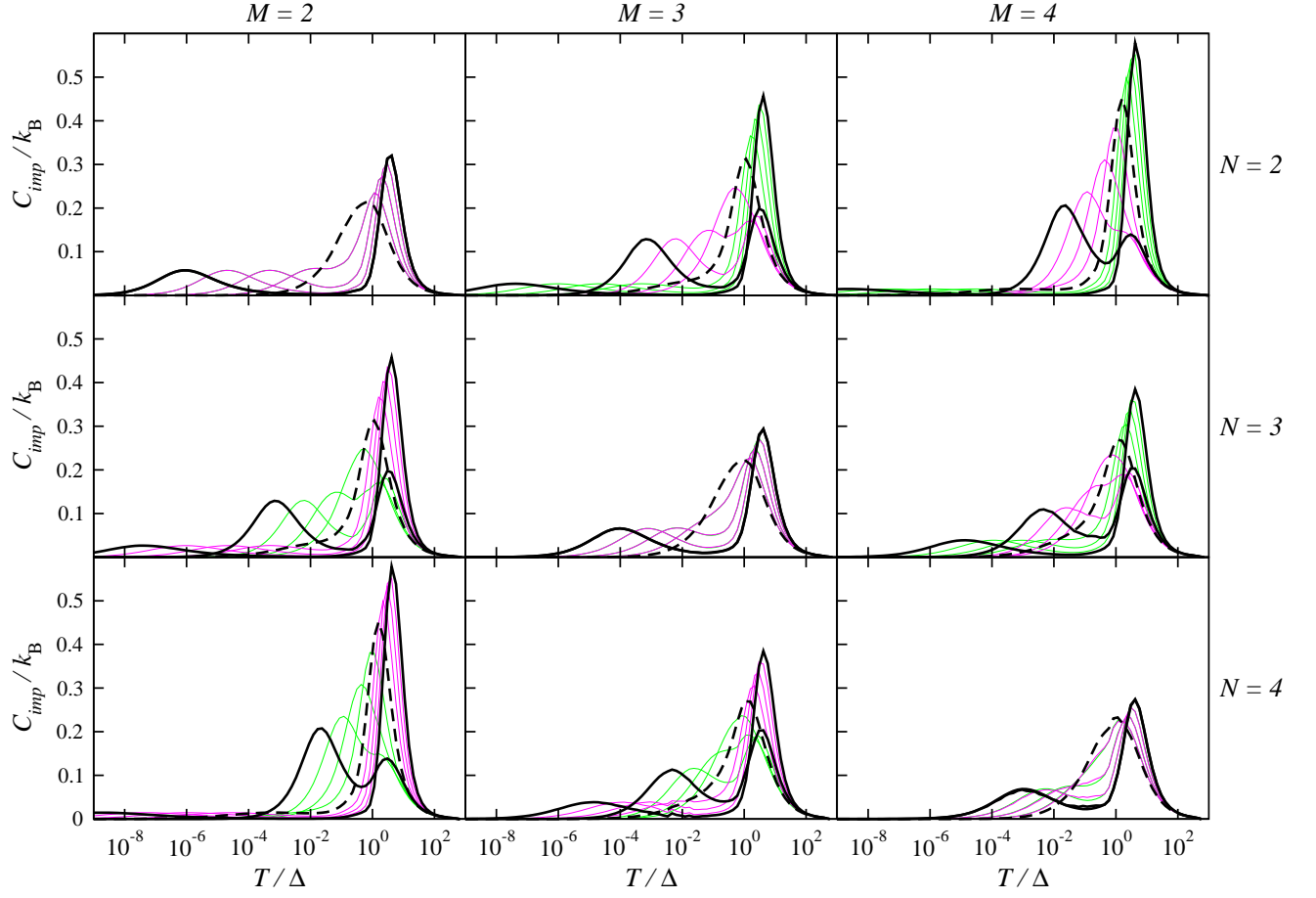


FIG. 5: Impurity specific heat as a function of temperature. The different curves correspond to: $\varepsilon/\Delta = 0$ (dashed lines); $\varepsilon/\Delta = \pm 2, \pm 4, \pm 6$ (light lines); and $\varepsilon/\Delta = \pm 8$ (dark solid lines). The different panels give the results for different values of N and M as indicated to the right and above, respectively. Curves for different signs of ε can be identified from the location of the Kondo anomaly or by comparison with the entropy plots.

in Sec. V A 3 c). Following the solid lines as the temperature lowers, the first quenching stage corresponds to the cross-over scale T_S and the impurity entropy attains the values $k_B \ln(N)$ or $k_B \ln(M)$ for $\varepsilon_s \ll \varepsilon_q$ or $\varepsilon_s \gg \varepsilon_q$ respectively. (As expected, in the case of $N = M$, the curves for different positive and negative values of ε are degenerate; on the other hand, for $N \neq M$, the curves for the same absolute values but opposite signs of ε are in precise correspondence upon exchange of the values of N and M).⁸⁰ These intermediate-regime plateaux correspond to the formation of a free local moment when $|\varepsilon| \gg \Delta$. As the temperature lowers further, following always the solid lines, the systems reach the Kondo cross-over scale, T_K , below which the entropy tends to the universal values $S_{\text{imp}}^0(N, M)$ characteristic of the different infrared non-Fermi liquid fixed points. This second quenching stage takes place as electrons in the different channels compete to screen the local moment of the intermediate regime. It is this dynamical *frustrated screening* process that is responsible for the non-trivial nature of the fixed point. In the mixed valence case, exemplified by the dashed line, the two cross-over energy scales are

of comparable magnitude and as a result the quenching of the entropy as the temperature is lowered happens on a single stage. Remarkably, the same limiting value of the impurity entropy is found also in this case; all consistent with the picture given above, that the infrared physics is governed by a line of fixed points (Sec. V A 3 c). In a previous work, we explored this explicitly (in the $N = M = 2$ case) using Boundary Conformal Field Theory and showed that the different points in the line are connected by an exactly marginal operator.³⁰

The results for the impurity contribution to the specific heat – obtained upon differentiation of the impurity entropy – are shown in Fig. 5. The different panels, and the different lines in each of them, follow the same conventions as in the entropy plots. In accordance with the generic two steps shape of the entropy (degenerate in the mixed valence case), the specific heat shows a general two humps structure (again degenerate for mixed valence). The lower temperature one is sometimes referred to in the experimental literature as the ‘Kondo anomaly’, and its location is correspondingly given by

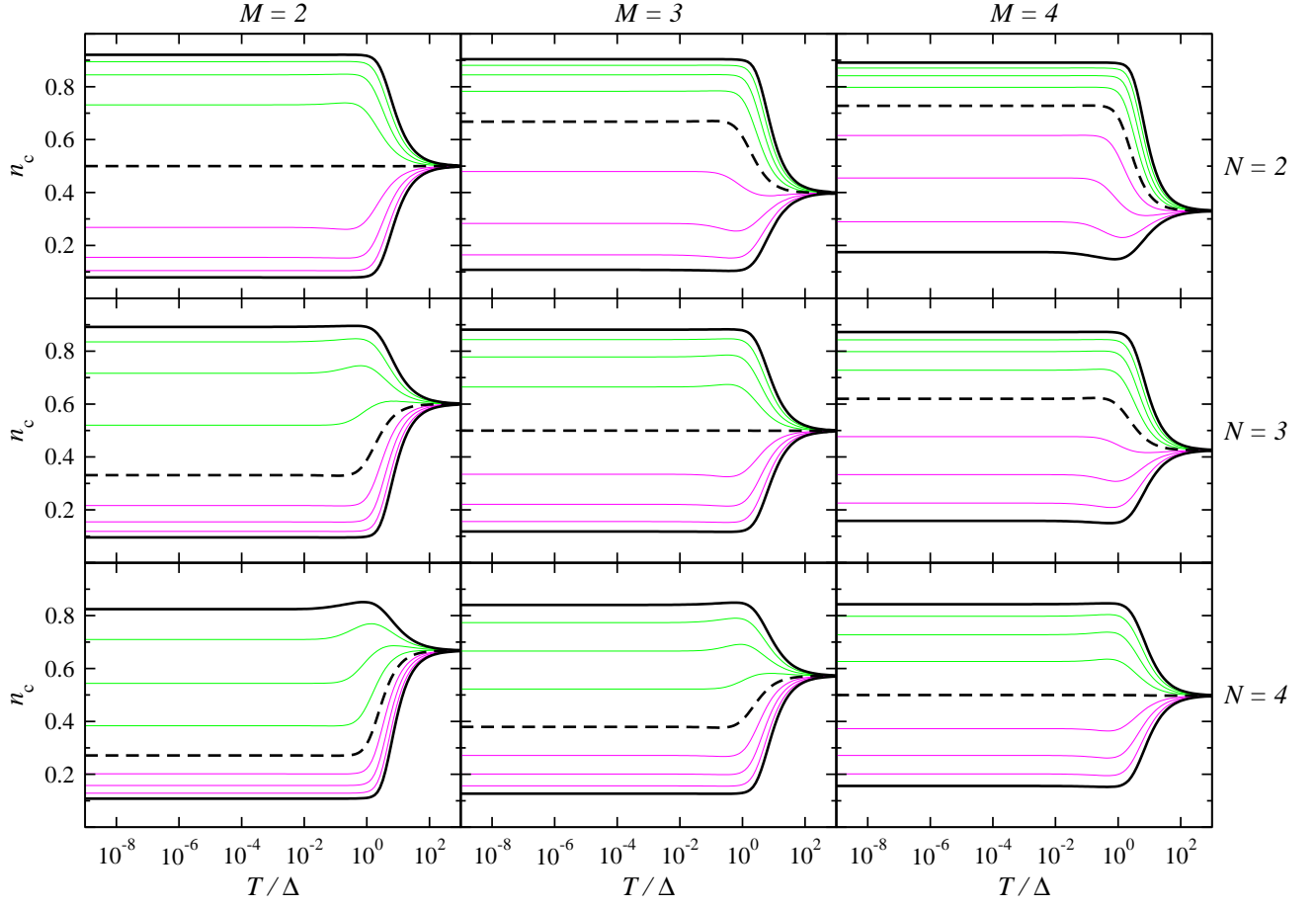


FIG. 6: Impurity charge valence as a function of temperature. The different curves correspond to: $\varepsilon/\Delta = 0$ (dashed lines); $\varepsilon/\Delta = \pm 2, \pm 4, \pm 6$ (light lines); and $\varepsilon/\Delta = \pm 8$ (dark solid lines). The different panels give the results for different values of N and M as indicated to the right and above, respectively. Curves for ε positive or negative are, respectively, below or above the $\varepsilon = 0$ line.

T_K . On the other hand, the higher temperature one is referred to as the ‘Schottky anomaly’ and its position is given by T_S . There is of course no new information in this figure as compared with the previous one, but it is the specific heat rather than the entropy or the free energy the quantity that is most often ‘directly’ accessible in the experiments.⁶¹

It is illustrative to look as well at the behavior as a function of temperature of the impurity charge valence, $n_{c,\text{imp}} = \sum_{\sigma} \langle f_{\sigma}^{\dagger} f_{\sigma} \rangle$. This is provided in Fig. 6 following identical conventions as in the plots for the entropy and the specific heat. As expected, in the high-temperature limit, the impurity valence approaches the values,

$$n_{c,\text{imp}}^{\infty}(N, M) = \frac{N}{N + M}$$

corresponding to the impurity Hilbert space fraction with ‘magnetic character’. This is an expression of the fact that, in that limit, all the impurity states are equiprobable. Subsequently, as the temperature crosses the

value T_S , the impurity charge valence changes and approaches rapidly what will be its zero temperature value, $n_{c,\text{imp}}^0(N, M)$. This change is at the origin of the Schottky anomaly in the specific heat. As it should be, the impurity approaches integer valence when $|\varepsilon| \gg \Delta$. The charge valence goes to zero in the *quadrupolar* limit of large and positive ε , and goes to one in the opposite, *magnetic* limit, of ε large but negative. The values of $n_{c,\text{imp}}^0$ for intermediate energy splittings are difficult to calculate and would constitute a good non-trivial test for approximate theories like those based on $(1/N)$ -expansions. Careful comparisons of NCA and NRG were carried out this way in the single-channel case,⁶² but for the multi-channel case the NRG calculations rapidly become very demanding for present day computational resources and this kind of comparisons were not done. Also, since the full cross-over takes place at the highest energy scale, the convergence of $n_{c,\text{imp}}^0$ should be relatively fast in NRG calculations. Thus in the future it might constitute a useful observable to monitor the progress of such computations by comparing with the exact solution.

As a check, we verified numerically that

$$n_{c,\text{imp}}^0(N, M)|_{\varepsilon} + n_{c,\text{imp}}^0(M, N)|_{-\varepsilon} = 1$$

so that, in particular, one finds that $n_{c,\text{imp}}^0(N, N)|_{\varepsilon=0} = 1/2$. The analytic form of $n_{c,\text{imp}}^0(N, M)$ can be computed using the zero temperature results of Sec. V A 1 (with the caveats given there for the case of $N \neq M$). For instance, in the two-channel case, we have

$$n_{c,\text{imp}}^0(2, 2) = \frac{2}{\pi} \int_{-\infty}^{+\infty} \int_{-\infty}^0 \frac{z \, dz}{\cosh \left[\frac{\pi}{2\Delta} (x - z) \right]} \times \frac{\mu - \varepsilon + x}{\left[(\mu - \varepsilon + x)^2 + 4\Delta^2 \right]^2} dx$$

$$\longrightarrow \begin{cases} \approx 1 & \text{for } \varepsilon \ll -\Delta \\ = \frac{1}{2} & \text{for } \varepsilon = 0 \\ \approx 0 & \text{for } \varepsilon \gg \Delta \end{cases}$$

(where we reintroduced the chemical potential). The inner integral is related to ξ_{q2} and has an exact expression in terms of dilogarithms. It is interesting to observe how, for certain values of the energy splittings, the charge valence first increases and then decreases as a function of the lowering temperature (or *vice versa*) as it goes from $n_{c,\text{imp}}^\infty$ to $n_{c,\text{imp}}^0$. This behavior is already present in the case of single-channel degenerate Anderson impurities.⁶²

Before proceeding, let us add some remarks on the technical side. We calculated both the entropy and the specific heat by numerically differentiating the free energy computed using the TBA distributions obtained with the algorithm described in the section above. Numerical differentiation is a delicate procedure very susceptible to truncation and roundoff errors and in general sensitive to any noise in the original data. The specific heat is, since a second derivative is involved, rather sensitive to this type of errors (the discretization of the temperature plays an interrelated role as well). In the event of better accuracy being required, alternative ways of computing derived thermodynamic quantities are possible. One common procedure is to set up secondary sets of integral equations for the different derivatives of the TBA distributions (see, for instance, Ref. [56]). Once the original distributions are found, these equations can be solved to determine their derivatives. Using them one can calculate directly (or with a smaller number of numerical differentiations) the sought derived quantities. The procedure to solve these auxiliary sets of equations will be in general similar to that used for the original TBA equations; making the total computational effort increase accordingly.

We turn now to discuss the effects of external fields on the physics of the impurity. For the sake of simplicity

we restrict ourselves to the two-channel case ($N = M = 2$). Since magnetic and quadrupolar fields are *relevant* perturbations, the presence of any of them has important effects on the entropy. In fact these perturbations drive the system to a totally different – this time Fermi liquid – line of fixed points characterized by a zero value of the residual impurity entropy (cf. with the situation in the single-channel case). This is illustrated in Fig. 7 where the entropy as a function of temperature is shown for different values of energy splitting between doublets (ε) and quadrupolar field (h_q).

In the upper left panel of the figure we reproduce again the results for zero field. The curves with positive and negative ε coincide in this case (remember we are setting $\mu = 0$ in this discussion). As we go from high to low temperatures, the system crosses over from a state with entropy $S_{\text{imp}} = k_B \ln 4$ to one with entropy $S_{\text{imp}} = k_B \ln \sqrt{2}$. This second value is one of the hallmarks of the non-trivial non-Fermi liquid fixed point that governs the low energy physics of the model.¹⁶ In the next panel to the right we show the effect of turning on an external field. For $h_q/\Delta = 10^{-6}$ one observes that the positive- ε curves stay in an $S_{\text{imp}} = k_B \ln \sqrt{2}$ plateau for a very short temperature interval (that disappears altogether when the impurity energy splitting is sufficiently large) and a third quenching step of the entropy takes it to a zero value final state, indicative of a Fermi liquid fixed point. As the reader can observe across the different panels, the quenching to zero entropy of the large positive ε curves takes place when the temperature is lowered until it becomes of the same order of magnitude as the applied field ($T \sim h_q$).

On the other hand, the fate of the negative- ε curves becomes more evident as we increase the field further (see the middle two panels). In this case too, the non-Fermi liquid fixed point is unstable and the entropy goes to zero, but this takes place at much lower temperatures than for positive ε . What happens is that at low temperatures the splitting of the higher multiplet (that plays the role of the orbital channel in the usual multi-channel Kondo scenario) renders the model an effective spin-half single-channel exchange model in which the impurity is ‘exactly’ screened at low temperatures and the fixed point is a Fermi liquid.⁶³ Curves with intermediate values of ε interpolate continuously between these two behaviors very much in the way they did in the other cases that we discussed above.

As the field is increased and approaches the scale of the first stage of entropy quenching (*i.e.* T_S) and beyond, the different- ε curves start to collapse and the temperature of the cross-over transition moves up following the field (compare the last two panels in Fig. 7). The entropy is quenched in a single stage from $S_{\text{imp}} = k_B \ln 4$ to zero at the same time as the impurity charge valence goes from $n_{c,\text{imp}} = 1/2$ to zero.

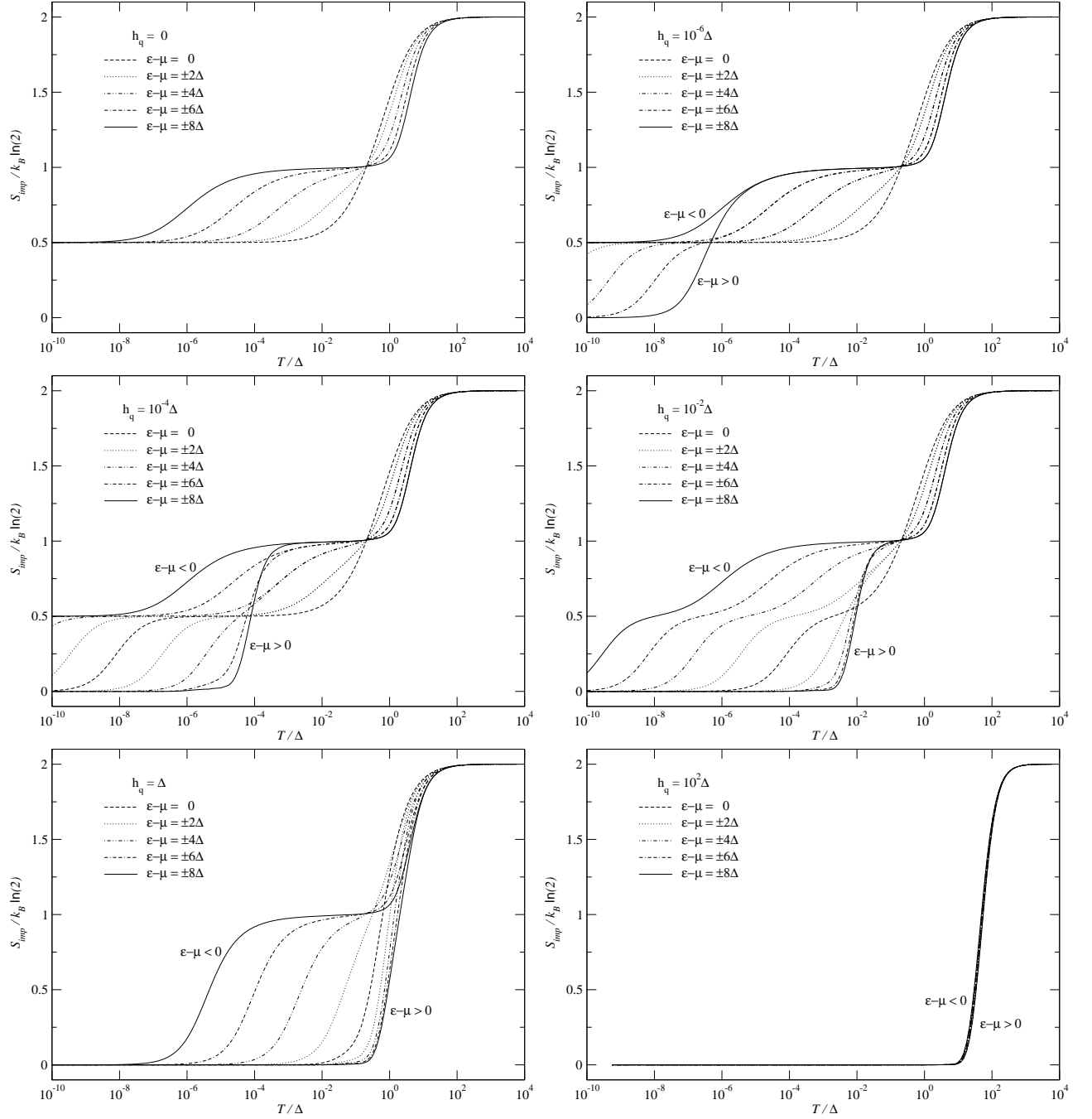


FIG. 7: Entropy as a function of temperature for various applied fields (we have chosen to consider quadrupolar flavor fields). The top-left panel corresponds to the zero field case. To the left of it and following downwards the field increases hundred-fold each time as $h_q = 10^{-6}\Delta, \dots, 10^2\Delta$. The values of ε are the same as in Fig. 4 (the chemical potential was reintroduced in the notation for this figure), and the top-left panels of both figures are in correspondence.

VI. SUMMARY AND OUTLOOK

We have carried out a detailed analysis of the multi-channel Anderson impurity model. We have demonstrated its integrability, discussed the details of the Bethe-Ansatz solution, and shown a number of illustrative results for the thermodynamics of the model.

The Bethe-Ansatz allows the study of the model on all energy scales, we proceed now to summarize our findings and to put them into context. We begin by discussing the low-temperature regime and the characterization of the low energy fixed point theory that corresponds to the microscopic model. We have identified the existence of a line of boundary critical fixed points that governs the low

energy physics of the impurity (illustrated in Fig. 8) and shown how it is related to the fixed point theory of the multi-channel Coqblin-Schrieffer model. In fact, every point in the line describes non-Fermi liquid physics. At the extreme ends ($|\varepsilon| \rightarrow +\infty$), the fixed point theory corresponds to an $SU_M(N)$ or $SU_N(M)$ Hamiltonian (in the sense of BCFT). For any finite value of ε , and in particular for all the values that correspond to the mixed valence region, the physics is given by a line of $SU_M(N) \oplus SU_N(M)$ theories. Along this line of fixed points the behavior, for instance, of the specific heat would be given by (cf. Ref. [46]),

$$C_{\text{imp}} \underset{N \neq M}{\sim} \lambda_c^2(\varepsilon) T + \lambda_s^2(\varepsilon) T^{\frac{2N}{N+M}} + \lambda_q^2(\varepsilon) T^{\frac{2M}{N+M}}$$

($N = M$ corresponding to the marginal case when both spin and quadrupolar sectors contribute $T \ln T$ leading temperature dependences; cf. Ref. [30]). The smallest exponent dominates as $T \rightarrow 0$, except possibly at the limit when $\varepsilon \rightarrow \pm\infty$ and $\lambda_s^2(\varepsilon)$ or $\lambda_q^2(\varepsilon)$ vanish, respectively. Thus these two limits do not commute when $f < n$ for the $SU_f(n)$ end of the fixed points line (with $n, f = N, M > 1$). Notice therefore, that as ε is varied along the line at small but finite temperature, the observed critical behavior will vary accordingly.

The same finite- T cross-over in non-Fermi liquid character (magnetic *vs.* quadrupolar) would manifest itself in a comparative study of both susceptibilities, whose expected leading low-temperature behaviors, after subtraction of asymptotic temperature-independent contributions, are:

$$\begin{cases} \chi_{\text{imp}}^s - \chi_0^s \underset{N \neq M}{\sim} \lambda_s^2(\varepsilon) T^{\frac{N-M}{N+M}} \\ \chi_{\text{imp}}^q - \chi_0^q \underset{N \neq M}{\sim} \lambda_q^2(\varepsilon) T^{\frac{M-N}{N+M}} \end{cases}$$

(here $N = M$ is again the marginal case, for which $\ln T$ dependencies are expected). Set for instance ε in the quadrupolar regime, then the corresponding $\lambda_q^2(\varepsilon)$ is large while $\lambda_s^2(\varepsilon)$ can be arbitrarily small. However, one will still find that, for all finite values of ε , the spin susceptibility will eventually dominate over the quadrupolar one if it happens to carry the singular exponent (*i.e.* for $N < M$).

Note that the level with the lower degeneracy always dictates the physics at sufficiently low temperatures even if it is a very high-energy level. This may be surprising from the point of view of the Schrieffer-Wolff limit (see Sec. V A 3). Naively, one would expect that the effects of the energetically unfavorable level could be simply integrated out. This is not always the case. When the degeneracy of this level is the smaller one, it will end up dominating at sufficiently low T (as long as $|\varepsilon|$ remains finite).⁸¹ In other words, discarding the energetically unfavorable yet less degenerate configuration also eliminates the frustration that is induced in the bulk electrons when they try to screen the virtual moment of such an excited state; but it is this frustration that would have been responsible for the appearance of singular exponents in the impurity thermodynamics.

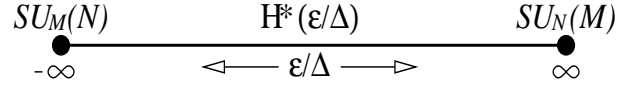


FIG. 8: Schematic representation of the line of fixed points.

This picture might help shed light upon some of the unexplained and sometimes contradictory results observed in the experiments.^{2,5} In particular, interesting possibilities are open up for better understanding of the intermediate-to-low temperature phase of certain heavy fermion compounds, inespically those believed to be near mixed valence (the list is rather large, for an example see below).

Thus far we discussed the low-temperature regime (FP – dominated by the line of *fixed points*). We have also studied in detail the other regimes: the high-temperature valence fluctuation regime (FV) and the intermediate local moment regimes (LMM and LQM) — the initialisms refer to the names used in Fig. 2. We identified the two energy scales (T_s and T_q) associated with the spin and quadrupolar degrees of freedom, that cross each other in the intermediate valence region ($|\varepsilon| \lesssim \Delta$) and interchange roles as the high-temperature (T_H) and low-temperature (T_L) scales that indicate the transition zones among different regimes. In the intermediate valence region the two scales ‘coincide’, indicating the direct transition between the high- and the low-temperature behaviors. The system never develops a local moment, but goes directly into the low-temperature, multi-channel Kondo like, non-Fermi liquid phase governed by the corresponding fixed points. In all the cases, *i.e.* for all values of ε , the fixed points are unstable to the application of an external field acting either on the magnetic or the quadrupolar degrees of freedom.

In subsequent work we intend to use the results presented here to analyze the different multi-channel scenarios for certain heavy-fermion compounds like $U_{1-x}\text{Th}_x\text{Be}_{13}$.^{23,64} It was shown that the two-channel Anderson model is not sufficient to account for the relevant number of impurity degrees of freedom required to explain the available specific heat measurements.²⁹ More complicated impurity models, like for instance an $SU(2) \otimes SU(5)$ model in the presence of crystal field splittings, hold a considerable promise in that respect.^{29,65}

Acknowledgments

During the different stages of this work, we enjoyed discussions with F. B. Anders, P. Coleman, T. Costi, T. Giamarchi, A. Jerez, H. Johannesson, H. R. Krishnamurthy, J. Kroha, A. Rosch, A. Schiller, N. Shah, and P. Wölfle. One of the authors was partly supported by the Swiss National Science Foundation through MaNEP.

APPENDIX A: QUANTUM INVERSE SCATTERING METHOD

In the following we will skip the details (and assume them known) of the standard case of models with $SU(2)$ internal symmetry, and refer the reader to the presentation given in the ICTP lectures by one of the authors.⁴⁰ We will adopt a notation very similar, though not identical, to the one in those lectures.⁸² We will discuss directly the case of $SU(3)$ symmetry conveniently generalized to the situation when both ‘particles’ and ‘antiparticles’ are present. This generalization is required to solve the eigenvalue problem of the multi-channel Anderson model (the standard *Nested Bethe-Ansatz* (NBA) as discussed in the literature, see for instance Ref. [66], does not suit this case), and was done before only for $SU(3)$ spin chains.^{67,68} Finally, we will close the appendix with the generalization to the case of $SU(N)$ symmetry.

1. Models with $SU(3)$ Symmetry, Impurities, and Periodic Boundary Conditions

Let us consider an integrable model with $SU(3)$ symmetric scattering matrices given by,

$$S_{jn \neq 0} = \frac{(\alpha_j - \alpha_n) \mathbf{I}_{jn} + ic \mathbf{P}_{jn}}{(\alpha_j - \alpha_n) + ic} = S_{jn}(\alpha_j - \alpha_n)$$

$$S_{j0} = \mathbf{I}_{j0} + \frac{e^{-i\delta(\alpha_j - \alpha_0)} - 1}{3} \mathbf{Q}_{j0} = S_{j0}(\alpha_j - \alpha_0) .$$

We choose to consider a case where S_{j0} has a different structure than $S_{jn \neq 0}$. In particular we consider the kind of impurity S-matrix that arises in the flavor sector of the three-channel Anderson model. The parameters α_j, α_0 are arbitrary at this point, and will be chosen later to be those that specify the multi-channel Anderson model. The eigenvalue problem given in terms of the above S-matrices is not tractable with the standard NBA formalism; we develop below the required extensions.

a. Monodromy Matrix

As a first step we define a matrix that captures the monodromy conditions of our eigenvalue problem and use its transfer matrix to rewrite the problem:

$$\Xi_A(\alpha) = S_{AN}(\alpha - \alpha_N) \dots S_{A1}(\alpha - \alpha_1) S_{A0}(\alpha - \alpha_0)$$

(this is equivalent to adding an auxiliary extra particle $A = N + 1$). The purpose of the auxiliary space will be to allow us to conveniently organize the products of the S-matrices (see below). We define the *transfer matrix* as:

$$T(\alpha) = \text{tr}_A \Xi_A(\alpha)$$

where tr_A denotes taking the trace in the auxiliary space A , and it follows that

$$T(\alpha_j) = Z_j .$$

As the amplitudes \vec{A} should be simultaneous eigenvectors of all the eigenvalue problems Z_j , it is necessary and sufficient that $[Z_j, Z_l] = 0$. We can go further and require $[T(\alpha), T(\beta)] = 0$ for all values of α and β . This is guaranteed if there exists a matrix R such that,

$$R_{AB}(\alpha - \beta) \Xi_A(\alpha) \Xi_B(\beta) = \Xi_B(\beta) \Xi_A(\alpha) R_{AB}(\alpha - \beta)$$

we will refer to this identity as the *fundamental commutation relation* (FCR).

b. Fundamental Commutation Relations

By repeated application of the Yang-Baxter relations, it can be shown that the matrix

$$R_{AB}(\alpha) = S_{AB}(\alpha) = \frac{\alpha \mathbf{I}_{AB} + ic \mathbf{P}_{AB}}{\alpha + ic}$$

satisfies the FCR. If we write down the expression for the monodromy matrix explicitly in the auxiliary space, we have (using a notation that is convenient for the Nested Bethe-Ansatz):

$$\Xi(\alpha) = \begin{pmatrix} A(\alpha) & B^2(\alpha) & B^3(\alpha) \\ C^2(\alpha) & D^{22}(\alpha) & D^{23}(\alpha) \\ C^3(\alpha) & D^{32}(\alpha) & D^{33}(\alpha) \end{pmatrix}$$

$$T(\alpha) = A(\alpha) + D^{22}(\alpha) + D^{33}(\alpha) .$$

Fully expanding the FCR in the two auxiliary spaces, it can be seen, after some algebra, that the sub-matrix D verifies the corresponding FCR of the $SU(2)$ case,

$$R_{AB}^{(2)}(\alpha - \beta) D_A(\alpha) D_B(\beta) = D_B(\beta) D_A(\alpha) R_{AB}^{(2)}(\alpha - \beta)$$

with

$$R_{AB}^{(2)}(\alpha) = S_{AB}^{(2)}(\alpha) = \frac{\alpha \mathbf{I}_{AB}^{(2)} + ic \mathbf{P}_{AB}^{(2)}}{\alpha + ic} .$$

This means that Yang-Baxter is obeyed by the sub-matrix. Defining $u_\alpha = \frac{\alpha - ic}{\alpha}$ and $v_\alpha = \frac{ic}{\alpha}$, one can write the following commutation relations between different components of the monodromy matrix:⁸³

$$A_\alpha B_\beta^s = u_{\alpha - \beta} B_\beta^s A_\alpha + v_{\alpha - \beta} B_\alpha^s A_\beta$$

$$D_\alpha B_\beta^s = u_{\beta - \alpha} B_\beta^s D_\alpha S_{As}^{(2)} + v_{\beta - \alpha} B_\alpha^s D_\beta \mathbf{P}_{As}^{(2)}$$

$$B_\beta^s B_{\beta'}^{s'} = B_{\beta'}^{s'} B_\beta^s S_{ss'}^{(2)} .$$

They will be used extensively in what follows.

c. *Reference State or Pseudo-vacuum*

We use the following local basis for the individual Hilbert space of each particle (where the ‘anti-particle’ one is for the impurity Hilbert Space):

$$|u\rangle, |\bar{u}\rangle = \begin{pmatrix} 1 \\ 0 \\ 0 \end{pmatrix}; \quad |d\rangle, |\bar{d}\rangle = \begin{pmatrix} 0 \\ 1 \\ 0 \end{pmatrix}; \quad |s\rangle, |\bar{s}\rangle = \begin{pmatrix} 0 \\ 0 \\ 1 \end{pmatrix}$$

and we define the following *highest weight reference state* which we will use to construct the Fock Space for the problem:

$$|\omega\rangle = \left(\bigotimes_{n=1}^N |u\rangle_n \right) \otimes |\bar{s}\rangle_0 .$$

Using the definitions $a_\alpha = \frac{\alpha}{\alpha+ic}$ and $b_\alpha = \frac{ic}{\alpha+ic}$ we can write down explicitly the scattering matrices in auxiliary space and see how they act on the reference state. Using that information we find for the monodromy matrix:

$$\Xi(\alpha) |\omega\rangle = \begin{pmatrix} |\omega\rangle & * & * \\ 0 & \Delta''(\alpha) |\omega\rangle & * \\ 0 & 0 & \Delta'''(\alpha) |\omega\rangle \end{pmatrix}$$

with

$$\Delta''(\alpha) = \prod_{j=1}^N a(\alpha - \alpha_j)$$

$$\Delta'''(\alpha) = \frac{2 + e^{-i\delta(\alpha - \alpha_0)}}{3} \Delta''(\alpha) .$$

Notice, for later use, that $\Delta''(\alpha_j) = 0$. We define $\Delta(\alpha) = \Delta''(\alpha) + \Delta'''(\alpha)$. For the transfer matrix we find (verifying that the reference state is indeed an eigenstate of it),

$$T_\alpha |\omega\rangle = (A_\alpha + D_\alpha^{22} + D_\alpha^{33}) |\omega\rangle = (1 + \Delta_\alpha) |\omega\rangle .$$

d. *Descendant States*

We will construct descendant eigenstates from the reference eigenstate that constitutes the highest weight state of the largest possible representation. Let us consider a state obtained by acting with the linear combination of M *flavor-lowering* operators (where $X_{s_1 \dots s_M}$ is an arbitrary tensor):

$$|\vec{\beta}\rangle = \sum_{\{s_i\}} B^{s_1}(\beta_1) \dots B^{s_M}(\beta_M) X_{s_1 \dots s_M} |\omega\rangle .$$

Using the FCR we find (the nomenclature of *wanted* and *unwanted* terms is standard, and the same as in Ref. [40]),

$$A_\alpha |\vec{\beta}\rangle \Big|_{\text{wanted}} = \left(\prod_{n=1}^M u_{\alpha - \beta_n} \right) |\vec{\beta}\rangle$$

$$D_\alpha |\vec{\beta}\rangle \Big|_{\text{wanted}} = \left(\prod_{n=1}^M u_{\beta_n - \alpha} \right) \times$$

$$\times B_{\beta_1}^{s_1} \dots B_{\beta_M}^{s_M} D_\alpha S_{A s_M}^{(2)} \dots S_{A s_1}^{(2)} X_{s_1 \dots s_M} |\omega\rangle$$

$$\text{tr}_A D_\alpha |\vec{\beta}\rangle \Big|_{\text{wanted}} = \left(\prod_{n=1}^M u_{\beta_n - \alpha} \right) \times$$

$$\times B_{\beta_1}^{s_1} \dots B_{\beta_M}^{s_M} T_\alpha^{(2)} X_{s_1 \dots s_M} |\omega\rangle$$

where in the last line we made the following definitions:

$$\Xi^{(2)}(\alpha) = D_\alpha S_{A s_M}^{(2)} \dots S_{A s_1}^{(2)}$$

$$T^{(2)}(\alpha) = \text{tr}_A \Xi^{(2)}(\alpha) .$$

Let us define the *reduced* monodromy matrix,

$$\tilde{\Xi}^{(2)}(\alpha) = S_{A s_M}^{(2)}(\alpha - \beta_M) \dots S_{A s_1}^{(2)}(\alpha - \beta_1) \equiv$$

$$\equiv \begin{pmatrix} \tilde{A}(\alpha) & \tilde{B}(\alpha) \\ \tilde{C}(\alpha) & \tilde{D}(\alpha) \end{pmatrix}$$

written in the *reduced* auxiliary space, and whose elements act only on the space of indexes $\{s_i\}$ (i.e. that spanned by all the possible $X_{s_1 \dots s_M}$). Notice that the elements of $\tilde{\Xi}^{(2)}$ and those of D commute with each other. We write down their ‘combined’ product explicitly:

$$\Xi_\alpha^{(2)} = D_\alpha \tilde{\Xi}_\alpha^{(2)} = \begin{pmatrix} A_\alpha^{(2)} & B_\alpha^{(2)} \\ C_\alpha^{(2)} & D_\alpha^{(2)} \end{pmatrix} .$$

Since both D and $\tilde{\Xi}^{(2)}$ satisfy the Yang-Baxter relations, we have a new set of FCR that are obeyed:

$$R_{AB}^{(2)}(\alpha - \beta) \Xi_A^{(2)}(\alpha) \Xi_B^{(2)}(\beta) =$$

$$= \Xi_B^{(2)}(\beta) \Xi_A^{(2)}(\alpha) R_{AB}^{(2)}(\alpha - \beta) .$$

The eigenvalue we are seeking involves more than a particular realization of the auxiliary tensor $X_{s_1 \dots s_M}$ (cf. with the NBA formalism). We can define a highest weight reference state for the space of $\{s_i\}$ in the standard way (notice that $\tilde{\Xi}^{(2)}$ is the usual monodromy matrix that appears in the $SU(2)$ case). We therefore consider the ‘combined’ reference state

$$|\omega\rangle_2 = |\tilde{\omega}\rangle |\omega\rangle \quad \text{with} \quad |\tilde{\omega}\rangle = \bigotimes_{n=1}^M |\uparrow\rangle_n$$

given by the direct product of a reference state in the space of indexes and $|\omega\rangle$ the previously defined reference state. In particular we have:

$$\tilde{\Xi}_\alpha^{(2)} |\tilde{\omega}\rangle = \begin{pmatrix} |\tilde{\omega}\rangle & * \\ 0 & \tilde{\Delta}_\alpha |\tilde{\omega}\rangle \end{pmatrix}$$

with $\tilde{\Delta}_\alpha = \prod_{n=1}^M a(\alpha - \beta_n)$. We can act on $|\omega\rangle_2$ with the ‘combined’ monodromy matrix:

$$\Xi_\alpha^{(2)} |\omega\rangle_2 = \begin{pmatrix} \Delta_\alpha'' |\omega\rangle_2 & * \\ 0 & \tilde{\Delta}_\alpha \Delta_\alpha''' |\omega\rangle_2 \end{pmatrix}.$$

Choosing the reference state $|\tilde{\omega}\rangle$ is equivalent to considering only B^2 ’s and no B^3 ’s when building eigenstates. This is the trivial case when the electrons do not hybridize with the impurity (we want instead to include non-trivial eigenstates involving some B^3 ’s as well). In the more general case that concerns us we write instead (inspired by the form of the *unwanted terms*):

$$\begin{aligned} |\vec{\beta}, \vec{\gamma}\rangle &= \sum_{\{s_i\}} B_{\beta_1}^{s_1} \dots B_{\beta_M}^{s_M} \left[B_{\gamma_1}^{(2)} \dots B_{\gamma_{M'}}^{(2)} |\omega\rangle_2 \right]_{s_1 \dots s_M} \equiv \\ &\equiv B_{\beta_1}^{s_1} \dots B_{\beta_M}^{s_M} |\vec{\gamma}\rangle. \end{aligned}$$

Let us denote by t_α the eigenvalue of $T(\alpha)$ and by $t_\alpha^{(2)}$ the eigenvalue of $T^{(2)}(\alpha) = A_\alpha^{(2)} + D_\alpha^{(2)}$. We need to solve the auxiliary eigenvalue subproblem:

$$T_\alpha^{(2)} |\vec{\gamma}\rangle = t_\alpha^{(2)} |\vec{\gamma}\rangle$$

(notice that both $T_\alpha^{(2)}$ and $|\vec{\gamma}\rangle$ are, although it is not explicitly indicated, functions of $\vec{\beta}$). Using the results from the $SU(2)$ case we write down the *wanted* terms:

$$\begin{aligned} A_\alpha^{(2)} |\vec{\gamma}\rangle \Big|_{\text{wanted}} &= \Delta_\alpha'' \left(\prod_{p=1}^{M'} u_{\alpha - \gamma_p} \right) |\vec{\gamma}\rangle \\ D_\alpha^{(2)} |\vec{\gamma}\rangle \Big|_{\text{wanted}} &= \tilde{\Delta}_\alpha \Delta_\alpha''' \left(\prod_{p=1}^{M'} u_{\gamma_p - \alpha} \right) |\vec{\gamma}\rangle \end{aligned}$$

and also the generic form of the *unwanted* ones:

$$\begin{aligned} A_\alpha^{(2)} |\vec{\gamma}\rangle \Big|_{\text{unwanted}} &= \\ &= \Delta_\alpha'' v_{\alpha - \gamma_q} \left(\prod_{p \neq q}^{M'} u_{\gamma_q - \gamma_p} \right) |\alpha \gamma_1 \dots \hat{\gamma}_q \dots \gamma_{M'}\rangle \end{aligned}$$

$$\begin{aligned} D_\alpha^{(2)} |\vec{\gamma}\rangle \Big|_{\text{unwanted}} &= \\ &= \tilde{\Delta}_{\gamma_q} \Delta_\alpha''' v_{\gamma_q - \alpha} \left(\prod_{p \neq q}^{M'} u_{\gamma_p - \gamma_q} \right) |\alpha \gamma_1 \dots \hat{\gamma}_q \dots \gamma_{M'}\rangle. \end{aligned}$$

The cancellation of the *unwanted* terms gives a first set of auxiliary conditions:

$$\prod_{p \neq q}^{M'} \frac{\gamma_q - \gamma_p - ic}{\gamma_q - \gamma_p + ic} = \frac{\gamma_q - \alpha_0 + i\frac{c}{2}}{\gamma_q - \alpha_0 + i\frac{3}{2}c} \prod_{n=1}^M \frac{\gamma_q - \beta_n}{\gamma_q - \beta_n + ic}$$

whereas the *wanted* terms give the auxiliary eigenvalue:

$$t_\alpha^{(2)} = \Delta_\alpha'' \left(\prod_{p=1}^{M'} u_{\alpha - \gamma_p} \right) + \Delta_\alpha''' \tilde{\Delta}_\alpha \left(\prod_{p=1}^{M'} u_{\gamma_p - \alpha} \right)$$

(notice that, since $\Delta_{\alpha_j}'' = 0$, the auxiliary eigenvalues vanish, *i.e.* $t_{\alpha_j}^{(2)} = 0$).

Having solved the auxiliary nested problem we can go back to the original eigenvalue problem that we are trying to solve. The combined *wanted* terms are:

$$T_\alpha |\vec{\beta}, \vec{\gamma}\rangle \Big|_{\text{wanted}} = B_{\beta_1}^{s_1} \dots B_{\beta_M}^{s_M} \left[\left(\prod_{n=1}^M u_{\alpha - \beta_n} \right) + \left(\prod_{n=1}^M u_{\beta_n - \alpha} \right) t_\alpha^{(2)} \right] |\vec{\gamma}\rangle = t_\alpha |\vec{\beta}, \vec{\gamma}\rangle.$$

And we find that the eigenvalues of $Z_j = T_{\alpha_j}$ read as

$$z_j = t_{\alpha_j} = \prod_{n=1}^M u_{\alpha_j - \beta_n} = \prod_{n=1}^M \frac{\alpha_j - \beta_n - ic}{\alpha_j - \beta_n}.$$

We are only left with the task of taking care of the *unwanted* terms. Generic ones read:

$$A_\alpha |\vec{\beta}, \vec{\gamma}\rangle \Big|_{\text{unwanted}} = A_\alpha \left(B_{\beta_n}^{s_n} B_{\beta_1}^{s_1} \dots \widehat{B_{\beta_n}^{s_n}} \dots B_{\beta_M}^{s_M} \right) \left(S_{s_1 s_n}^{(2)} \dots S_{s_{n-1} s_n}^{(2)} \right) |\vec{\gamma}\rangle$$

$$= v_{\alpha-\beta_n} \left(\prod_{m \neq n}^M u_{\beta_n-\beta_m} \right) \left(B_{\alpha}^{s_n} B_{\beta_1}^{s_1} \dots \widehat{B_{\beta_n}^{s_n}} \dots B_{\beta_M}^{s_M} \right) \left(S_{s_1 s_n}^{(2)} \dots S_{s_{n-1} s_n}^{(2)} \right) |\vec{\gamma}\rangle$$

and

$$\begin{aligned} D_{\alpha} \left| \vec{\beta}, \vec{\gamma} \right\rangle \Big|_{\text{unwanted}} &= D_{\alpha} \left(B_{\beta_n}^{s_n} B_{\beta_1}^{s_1} \dots \widehat{B_{\beta_n}^{s_n}} \dots B_{\beta_M}^{s_M} \right) \left(S_{s_1 s_n}^{(2)} \dots S_{s_{n-1} s_n}^{(2)} \right) |\vec{\gamma}\rangle \\ &= v_{\beta_n-\alpha} \left(\prod_{m \neq n}^M u_{\beta_m-\beta_n} \right) \left(B_{\alpha}^{s_n} B_{\beta_1}^{s_1} \dots \widehat{B_{\beta_n}^{s_n}} \dots B_{\beta_M}^{s_M} \right) \left(S_{s_1 s_n}^{(2)} \dots S_{s_{n-1} s_n}^{(2)} \right) D_{\beta_n} \Xi_{\beta_n}^{(2)} |\vec{\gamma}\rangle \end{aligned}$$

so that

$$\text{tr}_A D_{\alpha} \left| \vec{\beta}, \vec{\gamma} \right\rangle \Big|_{\text{unwanted}} = t_{\beta_n}^{(2)} v_{\beta_n-\alpha} \left(\prod_{m \neq n}^M u_{\beta_m-\beta_n} \right) \left(B_{\alpha}^{s_n} B_{\beta_1}^{s_1} \dots \widehat{B_{\beta_n}^{s_n}} \dots B_{\beta_M}^{s_M} \right) \left(S_{s_1 s_n}^{(2)} \dots S_{s_{n-1} s_n}^{(2)} \right) |\vec{\gamma}\rangle .$$

Since $\tilde{\Delta}_{\beta_n} = 0$, we have the following expression for the eigenvalue of the auxiliary problem: $t_{\beta_n}^{(2)} = \Delta_{\beta_n}'' \left(\prod_{p=1}^{M'} u_{\beta_n-\gamma_p} \right)$. Combining the two contributions to the same *unwanted* term and asking that it should vanish, we find a second set of auxiliary conditions:

$$\prod_{m \neq n}^M \frac{\beta_n - \beta_m - ic}{\beta_n - \beta_m + ic} = \prod_{j=1}^N \frac{\beta_n - \alpha_j}{\beta_n - \alpha_j + ic} \prod_{p=1}^{M'} \frac{\beta_n - \gamma_p - ic}{\beta_n - \gamma_p} .$$

e. Bethe-Ansatz Equations

Let us collect the different equations, rearrange them and highlight the final result. Recalling that $z_j = e^{-ik_j L}$ and performing the standard shift $\beta_n = \Lambda_n^{(1)} - i\frac{c}{2}$, we write the eigenvalue equation:

$$e^{ik_j L} = \prod_{n=1}^{M_1} \frac{\alpha_j - \Lambda_n^{(1)} + i\frac{c}{2}}{\alpha_j - \Lambda_n^{(1)} - i\frac{c}{2}}$$

and after shifting $\gamma_n = \Lambda_n^{(2)} - ic$, we write down also the auxiliary conditions:

$$\begin{aligned} \prod_{m \neq n}^{M_1} \frac{\Lambda_n^{(1)} - \Lambda_m^{(1)} - ic}{\Lambda_n^{(1)} - \Lambda_m^{(1)} + ic} &= \prod_{j=1}^N \frac{\Lambda_n^{(1)} - \alpha_j - i\frac{c}{2}}{\Lambda_n^{(1)} - \alpha_j + i\frac{c}{2}} \times \\ &\times \prod_{m=1}^{M_2} \frac{\Lambda_n^{(1)} - \Lambda_m^{(2)} - i\frac{c}{2}}{\Lambda_n^{(1)} - \Lambda_m^{(2)} + i\frac{c}{2}} \end{aligned}$$

and

$$\begin{aligned} \prod_{m \neq n}^{M_2} \frac{\Lambda_n^{(2)} - \Lambda_m^{(2)} - ic}{\Lambda_n^{(2)} - \Lambda_m^{(2)} + ic} &= \frac{\Lambda_n^{(2)} - \alpha_0 - i\frac{c}{2}}{\Lambda_n^{(2)} - \alpha_0 + i\frac{c}{2}} \times \\ &\times \prod_{n=1}^{M_1} \frac{\Lambda_n^{(2)} - \Lambda_n^{(1)} - i\frac{c}{2}}{\Lambda_n^{(2)} - \Lambda_n^{(1)} + i\frac{c}{2}} \end{aligned}$$

where we have taken $M_1 = M$ and $M_2 = M'$.

2. Generalization to Models with $SU(N)$ Symmetry

It is straightforward to generalize these results and write down the Bethe-Ansatz equations for the more general case of $SU(N)$ internal symmetry. We use the notation $M_0 = N_e$ for the number of electrons and $M_N = N_i$ ($=1$) for the *number of impurities*. We define $\Lambda_n^{(0)} = \alpha_n$ ($=k_n$) for the charge rapidities and $\Lambda_n^{(N)} = \varepsilon_n$ ($=\varepsilon$) (*i.e.* the *impurity rapidities*). Then we write the eigenvalue equations:

$$e^{ik_n L} = \prod_{m=1}^{M_1} \frac{\Lambda_n^{(0)} - \Lambda_m^{(1)} + i\frac{c}{2}}{\Lambda_n^{(0)} - \Lambda_m^{(1)} - i\frac{c}{2}}$$

and the nested auxiliary conditions:

$$\prod_{m \neq n}^{M_r} \frac{\Lambda_n^{(r)} - \Lambda_m^{(r)} - ic}{\Lambda_n^{(r)} - \Lambda_m^{(r)} + ic} = \prod_{\sigma=\pm 1} \prod_{m=1}^{M_{r+\sigma}} \frac{\Lambda_n^{(r)} - \Lambda_m^{(r+\sigma)} - i\frac{c}{2}}{\Lambda_n^{(r)} - \Lambda_m^{(r+\sigma)} + i\frac{c}{2}}$$

where the *rank* varies in the range $r = 1, \dots, N-1$.

a. Generalization to Models with $SU(N) \otimes SU(M)$ Symmetry

We start with the same auxiliary eigenvalue problem, but with the scattering matrices:

$$\begin{aligned} S_{jn \neq 0} &= \frac{(\alpha_j - \alpha_n) \mathbf{I}_{jn}^s - ic \mathbf{P}_{jn}^s}{(\alpha_j - \alpha_n) - ic} \frac{(\alpha_j - \alpha_n) \mathbf{I}_{jn}^q + ic \mathbf{P}_{jn}^q}{(\alpha_j - \alpha_n) + ic} \\ S_{j0} &= \mathbf{I}_{j0}^q + \frac{e^{-i\delta(\alpha_j - \alpha_0)} - 1}{M} \mathbf{Q}_{j0}^q . \end{aligned}$$

We choose to consider a case where S_{j0} acts non-trivially in the ‘channel’ degrees of freedom only (*i.e.* in ‘q-flavor’ space). This problem amounts to taking the one discussed above and adding an extra ‘isospin’ to it. The

monodromy matrix can be written as a direct product: $\Xi(\alpha) = \Xi^s(\alpha) \otimes \Xi^q(\alpha)$, and the transfer matrix becomes

$$T_\alpha = T_\alpha^s T_\alpha^q = (A_\alpha^s + D_\alpha^s) (A_\alpha^q + D_\alpha^q) .$$

The different steps go through as before and we get the Bethe-Ansatz Equations (BAE):

$$e^{ik_j L} = \prod_{n=1}^{M_1^s} \frac{\alpha_j - \Lambda_n^{s(1)} - i\frac{c}{2}}{\alpha_j - \Lambda_n^{s(1)} + i\frac{c}{2}} \prod_{m=1}^{M_1^q} \frac{\alpha_j - \Lambda_m^{q(1)} + i\frac{c}{2}}{\alpha_j - \Lambda_m^{q(1)} - i\frac{c}{2}}$$

with the conditions,

$$\prod_{m \neq n}^{M_r^s} \frac{\Lambda_n^{s(r)} - \Lambda_m^{s(r)} - ic}{\Lambda_n^{s(r)} - \Lambda_m^{s(r)} + ic} = \prod_{\sigma=\pm 1} \prod_{m=1}^{M_{r+\sigma}^s} \frac{\Lambda_n^{s(r)} - \Lambda_m^{s(r+\sigma)} - i\frac{c}{2}}{\Lambda_n^{s(r)} - \Lambda_m^{s(r+\sigma)} + i\frac{c}{2}}$$

$$\prod_{m \neq n}^{M_r^q} \frac{\Lambda_n^{q(r)} - \Lambda_m^{q(r)} - ic}{\Lambda_n^{q(r)} - \Lambda_m^{q(r)} + ic} = \prod_{\sigma=\pm 1} \prod_{m=1}^{M_{r+\sigma}^q} \frac{\Lambda_n^{q(r)} - \Lambda_m^{q(r+\sigma)} - i\frac{c}{2}}{\Lambda_n^{q(r)} - \Lambda_m^{q(r+\sigma)} + i\frac{c}{2}}$$

where for convenience we have used the definitions

$$\Lambda_n^{s,q(0)} = \alpha_n$$

$$\Lambda_1^{q(M)} = \alpha_0$$

and accordingly $M_0^{s,q} = N_e$, $M_M^q = N_i = 1$, and $M_N^s = 0$. One sees that the effect of the impurity enters via the auxiliary conditions for the *q-flavor-rapidities*.

The solution thus far was general. To specify it to our model we take $\alpha_j = k_j$ and $c = 2\Delta \equiv V^2$, and obtain the Bethe-Ansatz equations for the multi-channel Anderson impurity model. Removing the impurity (*i.e.* taking $M_M^q = 0$) one recovers the usual equations of the NBA formalism.⁶⁶

APPENDIX B: KERNELS AND IDENTITIES

In this appendix we collect a number of function and kernel definitions, and identities relating them, that are central to the writing, rewriting, and algebraic manipulation of the BAE and the equations of the TBA. Let us introduce the following notations aimed at lightening the writing of the BAE,

$$e_n(z) = \frac{z - in\Delta}{z + in\Delta}$$

$$e'_{nm}(z) = \prod_{\tau=1}^{\min\{m,n\}} e_{m+n+1-2\tau}(z)$$

$$e''_{nm}(z) = \prod_{\tau=1}^{\min\{m,n\}} e_{m+n-2\tau}(z)$$

$$e_{nm}(z) = \prod_{\sigma=\pm 1} e'_{nm+\sigma}(z) .$$

For the purpose of writing a continuum version of the BAE, we will need as well the derivatives of the logarithms of the above functions. We define the following

kernels:

$$K_n(z) = (2\pi i)^{-1} \partial_z \ln e_n(z) = \frac{1}{\pi} \frac{n\Delta}{z^2 + (n\Delta)^2}$$

plus the similar definitions

$$K_{nm}(z) = (2\pi i)^{-1} \partial_z \ln e_{nm}(z)$$

$$K'_{nm}(z) = (2\pi i)^{-1} \partial_z \ln e'_{nm}(z)$$

$$K''_{nm}(z) = (2\pi i)^{-1} \partial_z \ln e''_{nm}(z) .$$

These last three definitions are the basis to define the following ‘convolution’ kernels:

$$A_{nm}(z) = \delta_{n,m} \delta(z) + K_{nm}(z) =$$

$$= \sum_{\sigma=\pm 1} \sum_{\tau=1}^{\min\{m,n\}} K_{m+n+1+\sigma-2\tau}(z)$$

$$B_{nm}(z) = K'_{nm}(z) = \sum_{\tau=1}^{\min\{m,n\}} K_{m+n+1-2\tau}(z)$$

$$C_{nm}(z) = \delta_{n,m} \delta(z) + K''_{nm}(z) = \sum_{\tau=1}^{\min\{m,n\}} K_{m+n-2\tau}(z)$$

that are used extensively in the continuum formulation of the BAE.

b. Fourier Space Formalism

A great simplification in the algebraic manipulations is often achieved by working in terms of the Fourier transformed densities. Our convention will be as follows:

$$\tilde{\rho}(w) \equiv \mathcal{F}\{\rho(z)\}(w) = \int \rho(z) e^{-iwz} dz .$$

So that, for instance, the basic kernels adopt the simple form $\tilde{K}_n(w) = e^{-n\Delta|w|}$. Working in Fourier space is easy to see that different convolution kernels are simply related: $\tilde{B}_{n,m} = \tilde{K}_1 \tilde{C}_{n,m}$ and $\tilde{B}_{n,m} = \tilde{G} \tilde{A}_{n,m}$. Where one defines the ‘basic recursion kernel’,

$$\tilde{G}(w) = \frac{\tilde{K}_1(w)}{\tilde{K}_0(w) + \tilde{K}_2(w)} = \frac{1}{2 \cosh \Delta w}$$

$$G(z) = \mathcal{F}^{-1}\{\tilde{G}(w)\}(z) = \frac{1}{4\Delta \cosh \frac{\pi z}{2\Delta}}$$

that we call so because it enters many recursion relations connecting the different convolution kernels (for instance:⁴⁰ $\tilde{A}_{n,m} - \tilde{G} \tilde{A}_{n+1,m} + (1 - \delta_{n,1}) \tilde{G} \tilde{A}_{n-1,m} = \delta_{n,m}$ plus many others involving also the convolution kernels $\tilde{B}_{n,m}$ and $\tilde{C}_{n,m}$). All these relations are easy to prove in Fourier space.

c. General Recursion Kernels

The basic recursion kernel is ubiquitous in the TBA equations of all integrable models. For the case of the multi-channel Anderson model, we are also going to need the more general kernels:

$$\tilde{G}_m^{(N,M)} = \frac{\tilde{A}_{Nm}}{\tilde{A}_{MM}} = e^{-(N-M)\Delta|w|} \frac{\sinh(m\Delta w)}{\sinh(M\Delta w)}.$$

Of which the basic recursion kernel is a particular case, $G = G_1^{(2,2)}$. When $m = N$ some of these kernels are singular (have non-zero asymptotics in Fourier space). We regularize them according to

$$R G_m^{(N,M)}(\lambda) = G_m^{(N,M)}(\lambda) - \delta_{m,N} \delta(\lambda)$$

where we have expressed them, in direct space, in terms of the variable $\lambda = \pi z/2\Delta$. When carrying out numerical calculations, we will use the following explicit expressions for these kernels:

$$\begin{aligned} R G_m^{(N,M)} &= \\ &= \frac{1}{2\pi} \frac{1}{M\pi} \sum_{\substack{\sigma=\pm 1 \\ \tau=\pm 1}} \tau F\left(\delta_{N+\tau m,0} + \frac{N+\tau m}{2M} + i \frac{\sigma\lambda}{M\pi}\right) \end{aligned}$$

where $F(z) \equiv \partial_z \ln \Gamma(z)$ is the digamma function.

d. Rank Recursion Kernels

We also need, for intermediate manipulations, kernel operators that act on the rank indices. The basic one is $\tilde{G}^{rs} = \delta_s^r - (\delta_s^{r+1} + \delta_s^{r-1}) \tilde{G}$. Using it we can extend the convolution kernels as $\tilde{A}_{nm}^{rs} = \tilde{G}^{rs} \tilde{A}_{nm}$. A particularly useful derived kernel is the one given by the inverse: $R_X^{rs} \equiv [G^{-1} G^{sr}]^{-1}$, where the indices vary in the range $1, \dots, N-1$ or $1, \dots, M-1$ depending on the case ($X = N, M$). The explicit formula for this operator, in Fourier space, is

$$\tilde{R}_X^{rs} = \frac{\sinh[\min(r,s)\Delta w] \sinh[(X - \max(r,s))\Delta w]}{\sinh(\Delta w) \sinh(X\Delta w)}$$

and two particularly useful cases are given by the general recursion kernels:

$$\begin{aligned} R_M^{r1}(\lambda) &= G_{M-r}^{(M,M)}(\lambda) = \frac{\frac{1}{\pi M} \sin \frac{\pi(M-r)}{M}}{\cos \frac{\pi(M-r)}{M} + \cosh \frac{2\lambda}{M}} \\ R_N^{nN-1}(\lambda) &= G_n^{(N,N)}(\lambda) = \frac{\frac{1}{\pi N} \sin \frac{\pi n}{N}}{\cos \frac{\pi n}{N} + \cosh \frac{2\lambda}{N}} \end{aligned}$$

(these will be used in the determination of the Schrieffer-Wolff limit).

-
- ¹ F. Steglich *et al.*, Phys. Rev. Lett. **43**, 1892 (1979).
 - ² G. R. Stewart, Rev. Mod. Phys. **73**, 797 (2001).
 - ³ D. L. Cox, Phys. Rev. Lett. **59**, 1240 (1987), *Erratum: ibid.* **61**, 1527 (1988).
 - ⁴ G. R. Stewart, Z. Fisk, and J. O. Willis, Phys. Rev. B **28**, 172 (1983).
 - ⁵ D. L. A. Cox and A. Zawadowski, Adv. in Phys. **47**, 599 (1998).
 - ⁶ B. Andraka and A. M. Tsvelik, Phys. Rev. Lett. **67**, 2886 (1991).
 - ⁷ A. P. Ramirez *et al.*, Phys. Rev. Lett. **73**, 3018 (1994).
 - ⁸ F. G. Aliev *et al.*, Europhys. Lett. **32**, 765 (1995).
 - ⁹ A. C. Hewson, *The Kondo Problem to Heavy Fermions*, Cambridge University Press, Cambridge, England, 1993.
 - ¹⁰ P. Schlottmann, Phys. Rep. **181**, 1 (1989).
 - ¹¹ P. W. Anderson, Phys. Rev. **124**, 41 (1961).
 - ¹² P. B. Wiegmann, Phys. Lett. A **80**, 163 (1980).
 - ¹³ N. Kawakami and A. Okiji, Phys. Lett. A **86**, 483 (1981).
 - ¹⁴ P. Schlottmann, Phys. Rev. Lett. **50**, 1697 (1983).
 - ¹⁵ P. Schlottmann, Z. Phys. B **51**, 49 (1983).
 - ¹⁶ N. Andrei and C. Destri, Phys. Rev. Lett. **52**, 364 (1984).
 - ¹⁷ A. M. Tsvelik, J. Phys. C: Solid State Phys. **18**, 159 (1985).
 - ¹⁸ P. Schlottmann and P. D. Sacramento, Adv. Phys. **42**, 641 (1993).
 - ¹⁹ D. M. Cragg, P. Lloyd, and P. Nozières, J. Phys. C **13**, 803 (1980).
 - ²⁰ H. B. Pang and D. L. Cox, Phys. Rev. B **44**, 9454 (1991).
 - ²¹ I. Affleck and A. W. W. Ludwig, Nucl. Phys. **B360**, 641 (1991).
 - ²² A. Schiller, F. B. Anders, and D. L. Cox, Phys. Rev. Lett. **81**, 3235 (1998).
 - ²³ M. Koga and D. L. Cox, Phys. Rev. Lett. **82**, 2575 (1999).
 - ²⁴ F. B. Anders, Phys. Rev. B **71**, 121101(R) (2005).
 - ²⁵ D. L. Cox and A. E. Ruckenstein, Phys. Rev. Lett. **71**, 1613 (1993).
 - ²⁶ J. Kroha, P. Wölfe, and T. A. Costi, Phys. Rev. Lett. **79**, 261 (1997).
 - ²⁷ J. Kroha and P. Wölfe, Acta Phys. Pol. B **29**, 3781 (1998).
 - ²⁸ A. Tsuruta *et al.*, J. Phys. Soc. Jpn. **66**, 3528 (1997).
 - ²⁹ C. J. Bolech and N. Andrei, Phys. Rev. Lett. **88**, 237206 (2002).
 - ³⁰ H. Johannesson, N. Andrei, and C. J. Bolech, Phys. Rev. B **68**, 075112 (2003).
 - ³¹ H. Johannesson, C. J. Bolech, and N. Andrei, Phys. Rev. B **71**, 195107 (2005).
 - ³² J. Zinn-Justin and E. Brezin, C. R. Acad. Sci. **263**, 670 (1966).
 - ³³ C. N. Yang, Phys. Rev. Lett. **19**, 1312 (1967).
 - ³⁴ N. Andrei, K. Furuya, and J. H. Lowenstein, Rev. Mod. Phys. **55**, 331 (1983).
 - ³⁵ R. J. Baxter, *Exactly solved models in statistical mechanics*, Academic Press, London UK, 1982.
 - ³⁶ L. Faddeev and L. Takhtajan, Usp. Mat. Nauk. **34**, 15 (1979).
 - ³⁷ H. Bethe, Z. Phys. **71**, 205 (1931), in German.
 - ³⁸ M. Takahashi, Prog. Theor. Phys. **47**, 69 (1972).
 - ³⁹ D. Braak and N. Andrei, Nucl. Phys. **B542**, 551 (1999).
 - ⁴⁰ N. Andrei, in *Low-dimensional Quantum Field Theories*

- for *Condensed Matter Physicists*, edited by S. Lundquist, G. Morandi, and Y. Lu, World Scientific, Singapore and River Edge (N.J.), 1995, also available from arXiv:cond-mat/9408101.
- ⁴¹ C. N. Yang and C. P. Yang, *Journal of Mathematical Physics* **10**, 1115 (1969).
 - ⁴² M. Gaudin, *La fonction d'onde de Bethe*, Masson, 120 Bd. Saint-Germain, Paris, 1983.
 - ⁴³ M. Gaudin, *Phys. Rev. Lett.* **26**, 1301 (1971).
 - ⁴⁴ M. Takahashi, *Thermodynamics of one-dimensional solvable models*, Cambridge University Press, Cambridge UK, 1999.
 - ⁴⁵ M. Takahashi, *Prog. Theor. Phys.* **46**, 401 and 1388 (1971).
 - ⁴⁶ A. Jerez, N. Andrei, and G. Zaránd, *Phys. Rev. B* **58**, 3814 (1998).
 - ⁴⁷ P. Coleman and N. Andrei, *J. Phys. C: Solid State Phys.* **19**, 3211 (1986).
 - ⁴⁸ F. D. M. Haldane, *Phys. Rev. Lett.* **40**, 416 (1978), *Erratum: ibid.* **40**, 911 (1978).
 - ⁴⁹ B. Coqblin and J. R. Schrieffer, *Phys. Rev.* **185**, 847 (1969).
 - ⁵⁰ P. Nozières and A. Blandin, *J. Physique* **41**, 193 (1980).
 - ⁵¹ J. R. Schrieffer and P. A. Wolff, *Phys. Rev.* **149**, 491 (1966).
 - ⁵² H. U. Desgranges and J. W. Rasul, *Phys. Rev. B* **36**, 328 (1987).
 - ⁵³ A. M. Tsvelik, *Sov. Phys. JETP* **66**, 754 (1987).
 - ⁵⁴ V. T. Rajan, *Phys. Rev. Lett.* **51**, 308 (1983).
 - ⁵⁵ H. U. Desgranges and J. W. Rasul, *Phys. Rev. B* **32**, R6100 (1985).
 - ⁵⁶ T. A. Costi and G. Zaránd, *Phys. Rev. B* **59**, 12398 (1999).
 - ⁵⁷ G. Zaránd *et al.*, *Phys. Rev. B* **65**, 134416 (2002).
 - ⁵⁸ M. Takahashi and M. Shiroishi, *Phys. Rev. B* **65**, 165104 (2002).
 - ⁵⁹ C. Lanczos, *J. SIAM Numer. Anal. B* **1**, 86 (1964).
 - ⁶⁰ N. J. Higham, *Accuracy and Stability of Numerical Algorithms*, SIAM, Philadelphia, 1996.
 - ⁶¹ H. Rietschel *et al.*, *J. Mag. Mag. Mat.* **76&77**, 105 (1988).
 - ⁶² T. A. Costi, J. Kroha, and P. Wölfle, *Phys. Rev. B* **53**, 1850 (1996).
 - ⁶³ P. Schlottmann and K. J. B. Lee, *Phys. Rev. B* **52**, 6489 (1995).
 - ⁶⁴ N. Harrison *et al.*, *Phys. Rev. B* **63**, 081101(R) (2001).
 - ⁶⁵ N. Andrei and C. J. Bolech, On the multichannel-channel Anderson impurity model of uranium compounds, in *Concepts in Electron Correlation*, edited by A. C. Hewson and V. Zlatic, Kluwer Academic Publishers, 2003, also available from arXiv:cond-mat/0409616.
 - ⁶⁶ A. M. Tsvelik and P. B. Wiegmann, *Adv. Phys.* **32**, 453 (1983).
 - ⁶⁷ J. Abad and M. Ríos, *Phys. Rev. B* **53**, 14000 (1996).
 - ⁶⁸ J. Abad and M. Ríos, *J. Phys. A* **30**, 5887 (1997).
 - ⁶⁹ Indices α and σ transform according to the corresponding fundamental representation, the notation $\bar{\alpha}$ indicates that the index transforms instead with the complex conjugate representation.
 - ⁷⁰ The equality is in the sense of distributions (*i.e. almost everywhere*).
 - ⁷¹ We remind the reader that the electron gas with linear dispersion is highly degenerate. In other words, the two-electron free Hamiltonian $h_{1,2} = -i(\partial_1 + \partial_2)$ has as a general solution the wave function $\exp(ik_1x_1 + ik_2x_2)[A_{a_1a_2}\theta(x_1 - x_2) + (\mathbf{S}_{1,2}A)_{a_1a_2}\theta(x_2 - x_1)]$, with $\mathbf{S}_{1,2}$ arbitrary. As follows then from degenerate perturbation theory, one must choose already at zeroth-order the correct combination with respect to which to turn on a given perturbation. Our result corresponds to such a combination for the case when the perturbation is a multi-channel Anderson impurity.
 - ⁷² Notice that in order to achieve a formulation in terms of continuum distributions, the essential limit to be taken is $N_e \rightarrow \infty$. We remark that this is the same limit required in order to recover the field theory.
 - ⁷³ See Ref. [40] for a proof that it is a good approximation to restrict ourselves to the s-channel or q-channel highest weight states in the case of $SU(2)$; this proof can be extended to the general $SU(N)$ case.
 - ⁷⁴ We introduce the notation $\hat{\delta}_{n,1}$ that stands for $(1 - \delta_{n,1})$.
 - ⁷⁵ Here μ is the total chemical potential acting on the electrons, defined as $\mu = \mu_c + \mu_s + \mu_q$ with $\mu_s = \frac{1}{N} \sum_{n=1}^N h_{sn}$ and $\mu_q = \frac{1}{M} \sum_{m=1}^M h_{qm}$.
 - ⁷⁶ The notation in the subindex means: an arbitrary n such that $n < N$.
 - ⁷⁷ We remind the reader that, for the sake of simplicity, much of the discussion assumes $\mu = 0$.
 - ⁷⁸ Notice that $T_s \neq T_S$; these two scales only coincide, asymptotically, in the quadrupolar moment limit ($\varepsilon_s \gg \varepsilon_q$).
 - ⁷⁹ Alternatively, the whole discussion can be rephrased in terms of $\varepsilon - \mu$.
 - ⁸⁰ The different panels were nevertheless computed all independently as a check of the correctness of the program.
 - ⁸¹ Technically, in our case the SW transformation needs to be carried out carefully to the next order to see that the operators associated with the high-energy level mix with the low-energy ones and yield singular contributions when their associated degeneracy is the lower one.
 - ⁸² The differences stemming from the changed definition of the monodromy matrix: it will be the first index of the scattering matrices, rather than the second one, that shall be used as auxiliary space.
 - ⁸³ For reasons of brevity we shall henceforth use either notation: $A_\alpha \equiv A(\alpha)$, $u_\alpha \equiv u(\alpha)$, etc.